# Straining and advection contributions to the mixing process of the Patos Lagoon coastal plume, Brazil

**WILIAN C. MARQUES[1*], ELISA H. L. FERNANDES[1], OSMAR O. MOLLER[1]**

1. Universidade Federal do Rio Grande (FURG), Instituto de Oceanografia, Laboratório de Oceanografia Costeira e Estuarina, Caixa Postal 474, CEP 96200-0001 Rio Grande, RS, Brasil.

email: **wilian_marques@yahoo.com.br; dfsehf@yahoo.com.br; dfsomj@furg.br**

## Abstract

The Southern Brazilian Shelf (SBS) is a region influenced by freshwater, and the evolution of stratification can present important ecological consequences in this area. The aim of this paper was to investigate the importance of straining and advection processes that affect the stratification and de-stratification of the water column along the Southern Brazilian inner shelf, a region that is influenced by the Patos Lagoon coastal plume. The study was carried out through 3D numerical modeling experiments and the results were analyzed using the potential energy anomaly equation and wavelet analysis. Results showed that the potential energy anomaly showed strong variability over a time scale of several days and followed the wind pattern over the study region, and was accompanied by the monthly modulation of river discharge and remote effects associated with variability in oceanic circulation. However, the most important events in synoptic timescales occurred in periods shorter than 20 days and were coincident with the passage of meteorological systems over the study region. Straining and advection were the most important mechanisms for the

evolution of stratification in the adjacent coastal region. Nonlinearities and dispersion terms were as important as modulation effects, mainly during periods of high fluvial discharge. Close to the Patos Lagoon mouth, vertical advection explained most of the stratification evolution, due to the morphological characteristics in this region. In the frontal region and far field of the plume, two regions must be considered: the northeast part, which is characterized by the convergence of the coastal currents and ebb flows associated with the freshwater discharge that promote the domination of the cross-shore straining and advection, and the southwest part, which is controlled by the coastal currents that results in the domination by alongshore straining and advection and cross-shore advection terms. Close to the mouth of the Patos Lagoon, the occurrence of downward velocities generated downward displacement of the isopycnals, which decreases the potential energy anomalies, and vice versa. Near the frontal region, the anomalies were dependent on the intensity of the fluvial discharge. During moderate to high discharge events, the northeastward currents intensified mixing along-shore, which decreased the potential energy anomalies. In the same way, the southwestward currents intensified the spreading of freshwater and increased the stratification and the potential energy anomalies.

**Keywords:** coastal plume, Southern Brazilian Shelf, potential energy anomalies, numerical modeling, wavelet analysis

## 1. Introduction

Continental shelves influenced by freshwater inputs are diverse and highly productive environments mainly due to the availability of nutrients. Several studies

report the influence of continental discharge on the intensification of biological activities and maintenance of fishing stocks in coastal zones (Mann and Lazier, 1991). On the other hand, these regions are vulnerable and highly influenced by the introduction of both natural and anthropogenic continental materials. The continental waters and suspended matter enter the marine environment create remarkable features, namely coastal plumes, with density characteristics normally contrasting that of typical the coastal waters. The presence of plumes in coastal regions induces vertical and horizontal stratification and restrains the mixing processes. The continental discharge is also responsible for carrying fine sediments to the coastal areas. Depending on the dynamic conditions of the region, morphological features can be created along the coastal zones and modified over a wide range of spatial and temporal scales. Several studies present the importance of the contribution of suspended sediments in freshwater influenced regions to the maintenance of bed morphology (Wright and Nittouer, 1995; Wright and Friedrichs, 2006; Wang et al., 2007).

The stratified and de-stratified conditions have fundamental consequences for freshwater influenced regions, for example, Rabalais et al. (1999) reported that the stratification caused by Mississippi-Atchafalaya outflow prevents ventilation of lower-layer waters, allowing hypoxic conditions to develop on the continental shelf. The competition between stratification and mixing process can be investigated through analysis of potential energy. van Aken (1986) incorporated horizontal advection into the potential energy anomaly equation and showed its importance on the onset of seasonal stratification in certain areas of the North Sea. Burchard and Hofmeister (2008) illustrated the usefulness of the potential energy anomaly equation to investigate several process controlling stratification and de-stratification in

estuaries and coastal seas. de Boer et al. (2008) applied the same tool in order to analyze the importance of tidal straining and advection on the maintenance of the stratification in the Rhine River region. Earlier, the importance of tidal straining was investigated in Liverpool Bay by Simpson et al. (1990) and Sharples and Simpson (1993).

Thus, the fate and behavior of coastal plumes is controlled by linear and nonlinear processes, and their study can be accomplished through analysis of field data, remote sensing and numerical models. However, as the coastal circulation is naturally three dimensional and occurs in a broad range of spatial-temporal scales, it requires the consideration of baroclinic effects, considered through numerical modeling techniques (O'Donnel and Garvine, 1983; Royer and Emery, 1985; Chao and Boicourt, 1986; Chao, 1988a, 1988b; O'Donnell, 1990; Chapman and Lentz, 1993; Wong and Münchow, 1995; Kourafalou et al., 1996a, 1996b; Fong and Geyer, 2002; Morey et al., 2003; Piola et al., 2005; Xia et al., 2007; Guo and Valle-Levinson, 2007, among others).

Studies on the dynamics of plumes in the Southern Brazilian Shelf (SBS) (Figure 1A) are sparse. The SBS receives freshwater contributions from the La Plata River and the Patos Lagoon, which are advected by local coastal currents. The outer shelf is influenced by the Brazil and Malvinas western boundary currents (Castro and Miranda, 1998). At the southern boundary of the SBS, the La Plata River, the second main hydrographic basin of South America, discharges an annual mean of 22,000 $m^3$ $s^{-1}$ of freshwater in the coastal zone (Framiñan and Brown, 1996; Guerrero et al., 1997). Towards the north, the Patos Lagoon, located in the southernmost part of Brazil, is connected to the Atlantic Ocean by a single channel less than 1 km wide (Figure 1A). The principal rivers contributing at the north of the lagoon have a mean

annual discharge of 2400 $m^3$ $s^{-1}$ and exhibit discharge patterns similar to temperate regions that vary on inter-annual and inter-decadal timescales due to processes of climatic order (Marques and Moller, 2009). The influences of the South Atlantic anticyclone and anticyclones of polar origin contribute to the high spatial variability in wind circulation on synoptic timescales. The tides are mixed, with diurnal dominance, and these effects are restricted to the coastal zone and the estuarine region of the Patos Lagoon (Möller et al. 2001).

Previous numerical modeling studies on the SBS have low resolution in space and time (Piola et al., 2005; Soares et al., 2007a, 2007b). Therefore, these results were limited to considering only large scale coastal currents. Piola et al. (2005) investigated the importance of alongshore component of the wind stress controlling the seasonal variability of the La Plata plume. Soares et al. (2007a; 2007b) carried out realistic hydrodynamic simulations for the SBS and investigated the buoyancy-driven currents in the area and highlighted the contributions of the wind and tidal currents.

Previous studies on the dynamics of the Patos Lagoon coastal plume are even more limited due to the small scale of these processes. Zavialov et al. (2003) monitored the behavior of this plume during intense river runoff conditions by measuring salinity and temperature. Burrage et al. (2008) investigated the interaction of the Patos Lagoon coastal plume and the La Plata river buoyancy driven currents using airborne data. Marques et al. (2009) studied the physical forcing controlling the formation and behavior of the Patos Lagoon plume based on a three-dimensional hydrodynamic numerical model. These authors verified the influence of local wind action spreading the coastal plume along shore and promoting the stratification and mixing of the coastal waters. The contribution of each mechanism controlling the mixing of the adjacent coastal waters, however, is still unknown. Thus, the aim of this

paper was to investigate the importance of straining and advection increasing the understanding of modulation of stratification inside the Patos Lagoon coastal plume for each of its known physical modes using potential energy anomaly budgets.

This paper is organized as follows. The section 2 presents the methodology, explaining the numerical model used with their setting parameters, presenting the time-dependent dynamic equation for potential energy anomaly, as well as, the methods used to analyze the obtained results. In section 3 and 4 the verification of the modeled results is carried out using some field measurements. The obtained results are presented in section 5 and discussed in section 6. Some conclusions are presented in section 7.

## 2. Methodology

This study is based on the application of three dimensional hydrodynamic numerical models combined with field data measurements. Current velocity and salinity profiles observed in situ are used to verify the ability of the model to represent the physical processes of the study region. The potential energy anomaly equation and wavelet analysis are used to investigate the influence of different physical mechanisms that control stratification and mixing along the adjacent continental shelf.

### 2.1. The hydrodynamic numerical model

The TELEMAC SYSTEM, developed by ©EDF – *Laboratoire National d'Hydraulique et Environnement* of the *Company Eletricité de France (EDF)* is used for the hydrodynamic simulations. The TELEMAC3D model solves the Navier

Stokes equations by considering local variations in the free surface of the fluid, neglecting the density variations in the mass conservation equation, and considering the hydrostatic pressure and Boussinesq approximations in order to solve the motion equations. The model is based on the finite element techniques to solve the hydrodynamic equation (Hervouet, 2007).

The time step of 90 s and the Coriolis coefficient of -7.70 x $10^{-5}$ N $m^{-1}$ $s^{-1}$ (latitude 32ºS) were used in all the simulations. The horizontal turbulence process was performed using the Smagorinsky model. This closure turbulent model is generally used for maritime domains with large scale eddy phenomena, calculating the mixing coefficient by considering the size of the mesh elements and the velocity field (Smagorinsky, 1963). The mixing length model for buoyant jets was implemented to access the vertical turbulence process, giving a better representation of the stratification and the vertical mixing processes. This model takes into account density effects via a damping factor, which depends on the Richardson number, to calculate the vertical diffusion coefficients. According to Hervouet (2007), the use of traditional mixing length models lead to abnormal results in the case of outflows where dissipation was overestimated. To address this, Rodi (1984) proposed the mixing length model for buoyant jets that considered a mixing length scale of about 8% of the half-height of the jet, defined as the distance between the elevation of the jet axis and the height where velocity does not exceed 1% of its maximum value. Determining the half-height of the jet was necessary for this study and a value of 10 m was considered as the mixing length scale in all simulations.

### 2.2. The potential energy anomaly equation

Potential energy arguments were used in order to investigate the dominant processes influencing the stratification and mixing along the Southern Brazilian inner shelf. The potential energy anomaly equation is suitable for the analysis of results from three-dimensional numerical models or field measurements. de Boer et al. (2008) derived this equation using the Reynolds averaged advection-diffusion equation for density with sources and sinks, and obtained:

$$\frac{\partial \varphi}{\partial t} = \frac{g}{H}\int_{-h}^{\eta}\left[\tilde{u}\frac{\partial \overline{\rho}}{\partial x} + \tilde{v}\frac{\partial \overline{\rho}}{\partial y} + \bar{u}\frac{\partial \overline{\rho}}{\partial x} + \bar{v}\frac{\partial \overline{\rho}}{\partial y} + \tilde{u}\frac{\partial \tilde{\rho}}{\partial x} + \tilde{v}\frac{\partial \tilde{\rho}}{\partial y} - \frac{1}{H}\frac{\partial \overline{u}\overline{\rho}H}{\partial x} - \frac{1}{H}\frac{\partial \overline{v}\overline{\rho}H}{\partial y} + \frac{\partial \langle \rho' u' \rangle}{\partial x} + \frac{\partial \langle \rho' v' \rangle}{\partial y} + \frac{\partial \langle \rho' w' \rangle}{\partial z} + w\frac{\partial \rho}{\partial z} - \frac{1}{H}\left(\langle \rho' w' \rangle|_{s} - \langle \rho' w' \rangle|_{B}\right)\right] z dz - \frac{\varphi}{H}\frac{\partial H}{\partial t} - \left(\frac{g}{H}\right)\left[\tilde{\rho}(\eta)\eta\frac{\partial \eta}{\partial t}\right] \quad (1.1)$$

With:

$$\varphi = \frac{1}{H}\int_{-h}^{\eta}(\bar{\rho} - \rho) g z dz \quad (1.2)$$

Where: $\varphi$ is the potential energy anomaly; *t, x, y, z* represent the time and position coordinates, respectively; *ρ, u, v, w* represent the density and the components of velocity, respectively; $\overline{\rho}$, $\bar{u}$, $\bar{v}$ represent depth averaged values; $\tilde{\rho}$, $\tilde{u}$, $\tilde{v}$ represent the deviations from the depth mean values; *H* is the water depth; *g* is gravity acceleration; $\eta$ is the surface elevation. Here $\langle \rho' u' \rangle, \langle \rho' v' \rangle, \langle \rho' w' \rangle$ are the turbulent flux of mass in the *x*, *y* and *z* directions. Detailed information about the calculations can be found in Simpson et al. (1990), de Boer et al. (2008), and Burchard and Hofmeister (2008).

This equation represents the local variation of the potential energy anomaly on the left side. On the right side, the first and the second terms represent the cross shore and along shore straining of the density fields. The third and the fourth terms are

referred to as the cross shore and along shore advection of a vertical structure by the depth mean current. The fifth and the sixth terms represent the non linear interaction of density and flow deviations in the vertical direction. The seventh and eighth terms describe the effect of correlation over the vertical, between the velocity shear and the vertical variation of the horizontal gradient. These terms are just the depth averaged counterparts of the fifth and sixth ones. The ninth and tenth terms are the horizontal depth averaged dispersion terms. The eleventh term represents the effect of the vertical mixing on the density profile. The twelfth term is related to up- and downwelling processes. The thirteenth and fourteenth terms are the surface and bed turbulent fluxes. The fifteenth and the sixteenth terms are presented due to temporal changes in the water depth or the surface elevation.

In this work, the processes with shorter time scales (shorter than one day) were not investigated. Thus, all the turbulent terms were neglected. Considering the simplifications, the equation reduces to:

$$\frac{\partial \varphi}{\partial t} = \frac{g}{H}\int_{-h}^{\eta}\left[\tilde{u}\frac{\partial \tilde{\rho}}{\partial x} + \tilde{v}\frac{\partial \tilde{\rho}}{\partial y} + \bar{u}\frac{\partial \tilde{\rho}}{\partial x} + \bar{v}\frac{\partial \tilde{\rho}}{\partial y} + \tilde{u}\frac{\partial \bar{\rho}}{\partial x} + \tilde{v}\frac{\partial \bar{\rho}}{\partial y} - \frac{1}{H}\frac{\partial \overline{\tilde{u}\tilde{\rho}}H}{\partial x} - \frac{1}{H}\frac{\partial \overline{\tilde{v}\tilde{\rho}}H}{\partial y} + w\frac{\partial \rho}{\partial z}\right]z\,dz - \frac{\varphi}{H}\frac{\partial H}{\partial t} - \left(\frac{g}{H}\right)\left[\tilde{\rho}(\eta)\eta\frac{\partial \eta}{\partial t}\right] \tag{1.3}$$

Symbols were defined to represent each term in order to simplify in-text references. Considering the same order defined in the equation 1.3, each term is named by a letter with a subscript index, similar to de Boer et al. (2008), representing its position in the equation as:

$$\frac{\partial \varphi}{\partial t} = \frac{g}{H}\int_{-h}^{\eta}\left[S_x + S_y + A_x + A_y + N_x + N_y + C_x + C_y + W_z\right]z\,dz - B_H - B_\eta \tag{1.4a}$$

$$SUMT = \left(S_x + S_y + A_x + A_y + N_x + N_y + C_x + C_y + W_z\right) \quad (1.4b)$$

$$AS = \left(S_x + S_y + A_x + A_y\right) \quad (1.4c)$$

SUMT represents the sum of terms inside the integral (from $S_x$ to $W_z$). Previous studies reported these terms as the most important for controlling the changes in stratification of real systems (Burchard and Hofmeister, 2008; de Boer et al., 2008). AS represents the sum of straining and advective process. Similar to de Boer et al. (2008), two methods of analysis were adopted in this work. The first is the covariance analysis between an arbitrary term $\alpha$ of the equation (1.3) and the potential energy anomaly $\frac{\partial \varphi}{\partial t}$ calculated as:

$$cov\left(\alpha, \frac{\partial \varphi}{\partial t}\right) = \sum_{i=0}^{N-1}\left[\left(\alpha(i) - avg(\alpha)\right)\left(\frac{\partial \varphi}{\partial t}(i) - avg\left(\frac{\partial \varphi}{\partial t}\right)\right)\right] \quad (1.5a)$$

$$avg(\alpha) = \frac{1}{N}\sum_{i=0}^{N-1}\alpha(i) \quad (1.5b)$$

Where: $\alpha$ represents a term in equation (1.3), $i$ is a time step counter and $N$ is the number of time steps. The second method is a direct time series analysis at selected points along the Southern Brazilian inner shelf. The first method verifies the space component for the most important terms controlling the mixing process during the entire study period, while the second method investigates the temporal variability of the most important terms, verifying their importance as time evolves. The results obtained with the numerical model were used to identify the temporal variability of

the potential energy anomaly of the Patos Lagoon plume using wavelet analyses. The spectral content of the potential energy anomaly time series were analyzed using an adaptation of the Morlet wavelet method described by Torrence and Compo (1997).

### 2.3. The initial and boundary conditions of the numerical model

Initial conditions of salinity and temperature fields were prescribed for the TELEMAC3D model. Salinity and temperature fields were obtained from the OCCAM Project (*Ocean Circulation and Climate Advanced Modeling Project* *http://www.soc.soton.ac.uk*), and prescribed tri-dimensionally over the entire domain. Water levels of 0.4 m, about the mean value of the tides in the study region, and null velocity fields were prescribed as initial conditions in the entire domain. The salinity and temperature along the Patos Lagoon were initialized with spatially constant values of 0 and 20 ºC, respectively (Figures 2A and 2B). In the coastal area, the salinity and temperature fields represent the influence of the La Plata river discharge over the Southern Brazilian Shelf (Figure 2A) and the Brazil Current along the continental shelf at the northern oceanic boundary (Figure 2B).

The time series of river discharge from the rivers at the north of the lagoon were used to force the continental liquid boundary (Figure1B). According to Marques (2005), the Taquari and Jacuí rivers (tributaries of the Guaíba river) and the Camaquã river (Figure 1A) are the main tributaries of the Patos Lagoon. The river discharge data was provided by the Brazilian National Water Agency (*www.ana.gov.br, ANA*). The time series of river discharge used in this study ranged from January 1$^{st}$ 1998 to

November 18th 1999 (Figure 3). The higher discharge observed during the 1998 year indicates the influence of El Niño in the study area.

The tidal influence is prescribed at each nodal point of the oceanic boundary (Figure 1B) using the amplitude and phase of the five main tidal components of the study area (K1, M2, N2, O1, S2; Fernandes et al. 2004), obtained from the Grenoble Model (*FES95.2, Finite Element Solution – v.95.2*). The data were interpolated using a cubic interpolation method for the oceanic boundary. The tidal oscillation is represented as the sum of cosine functions calculated for each node of the oceanic boundary at each time step of the simulation.

The surface boundary of the model is forced with space and time variable winds from reanalysis (*National Oceanic & Atmospheric Administration–NOAA, www.cdc.noaa.gov/cdc/reanalysis*), which are prescribed at each nodal point of the mesh using a constant coefficient of wind influence of $1 \times 10^{-5}$. The data were obtained with a temporal resolution of 24 h. The meridional and zonal wind components were collected between 25ºS 42ºW and 38ºS 55ºW and later interpolated using a cubic interpolation method for the numerical domain. A similar methodology was adopted by Simionato et al. (2006a) when using the reanalysis data to model the barotropic circulation of the La Plata River mouth. The study region was influenced by the alternation of anti-cyclonic atmospheric systems, which induce the dominant wind in the north quadrant, and the intermittent south quadrant winds were associated with the passage of frontal systems. Figure 4 shows these wind patterns, as well as the spatial variability observed in this domain.

In order to represent the remote wind effect along the Southern Brazilian Shelf, low frequency water levels were prescribed at each nodal point of the oceanic boundary (Figure 1B). These represent the monthly variation of the water level and

this influence was represented by the direct imposition at the oceanic boundary. The influence of the coastal currents was implemented by prescribing the low frequency current velocity at each nodal point of the oceanic boundary (Figure 1B). The current velocity time series were implemented tri-dimensionally along the transversal boundaries of the model, representing the monthly variation of the current velocity along the Southern Brazilian Shelf. Data sets of water level and current velocity that were used as boundary conditions were obtained from the OCCAM Project and were interpolated using the cubic interpolation method. Figure 5 illustrates the water level and intensity of current velocity prescribed as boundary conditions on the surface layer in two different points along the oceanic boundary (see positions in figure 1B).

The influence of the buoyancy driven currents from the La Plata River was considered by prescribing a salinity time series at each nodal point along the oceanic boundary (Figure 1B). The heat balance between different water masses at the oceanic boundaries was simulated through the prescription of temperature time series. These data were obtained from the OCCAM Project, interpolated using the cubic interpolation method and prescribed tri-dimensionally along the entire oceanic boundary (Figure 1B). The heat exchange between the free surface of the model and the atmosphere was considered using air temperature data from the Reanalysis web page. These data have a temporal resolution of 24 h and the same procedure of interpolation applied to the wind was used for air temperature.

The water temperature in the free surface was determined according to heat exchange with the atmosphere under thermodynamic principles. A detailed description of the thermal power equation used into the TELEMAC3D as well as the radiation coefficient, convection of air close to the water and latent heat produced for evaporation of the water can be found in Hervouet (2007). Figure 6 presents the

salinity and temperature prescribed for oceanic boundary conditions in two different points of the superficial layer (see positions in Figure 1B). Figures 5 and 6 indicate the seasonal and annual variability imposed on the numerical simulation considering remote wind effects, low frequency contribution of the coastal currents, buoyancy terms and heat exchange along the Southern Brazilian Shelf.

## 3. Verification of the hydrodynamic results – 2008 year

Previous calibration exercises for the TELEMAC3D hydrodynamic model applied in the Southern Brazilian Shelf were presented by Marques et al. (2009) using current velocity and water levels. In order to verify the reproducibility of the model, results from a hydrodynamic simulation were compared with observed time series measurements at the coast and the estuarine area from August 2$^{nd}$ to September 22$^{nd}$ 2008. The observed current velocity time series were measured at the Praticagem Station and the inner continental shelf (Figure 1C) using an Acoustic Doppler Current Profiler (ADCP).

The comparison between the daily time series of calculated and observed current velocity (Figure 7A and 7B) at 3 m and 14 m depths indicate that the model can reproduce the real variability and trends of the velocity field in the estuarine region with some underestimation of the intensity. The comparison between the calculated and observed current velocity in the inner continental shelf (Figure 8) indicates that the model reproduces the signal trends. Some differences appear in the north/south bottom component after 900 hours (Figure 8C) and in the north/south superficial component (Figure 8A). This underestimation may be related to the use of

a spatially constant coefficient of wind influence in this study or due the use of Reanalysis low resolution data sets.

Flather (1976) suggested the guideline of variation for this coefficient according to the intensity of the wind. In fact, the influence of the wind depends on the roughness of the free surface, which is dependent on the wind and the fetch. On the other hand, some authors using the Reanalysis wind data sets observed some problems capturing the temporal and spatial variability of observed processes. Simionato et al. (2006a) carried out analysis using reanalysis data (24 h resolution) for the La Plata river region and also observed that the high intensity events were underestimated by up to 50% when compared with field data. Ruti et al. (2008) attributed to the low spatial resolution of Reanalysis data as the main source of errors in a comparison with analyzed wind fields over the Mediterranean basin. However, a general overview of this verification exercise indicates that, apart from the limitations in the data used to initialize and force the model, the calculated velocity time series satisfactorily represent the intensity and trends of the signals measured inside the estuary and in the inner continental shelf.

In order to quantify the reproducibility of the model, the method proposed by Sutherland (2001) was used. This method calculates the Root Mean Square Error (RMSE) between the observed and calculated time series. The calculated RMSE for the simulation period is presented in the lower right side of each figure. Results indicate that greater error occurring in the superficial layers of the estuarine region. The error in this region is approximately 0.21 and 0.25 m $s^{-1}$. In the inner continental shelf, the error is lower than 0.17 m $s^{-1}$, indicating better simulation of velocity by the model. Lag correlation analysis (Figure 9) were performed in order to indicate the strength and direction of a linear relationship between the calculated and observed

velocities. The results indicated zero lag between the variables in daily time scales and good correlation coefficients (r) greater than 0.65 for all the calculated velocities.

## 4. Verification of salinity results – October 26th 1998

The precision of the salinity profiles calculated by the model in the coastal zone was verified by comparing the results from the hydrodynamic simulation with field data from eight vertical profiles of conductivity, temperature and depth profiler (CTD) data collected near the estuarine mouth on October 26th 1998 (see positions in Figure 1C). The hydrodynamic simulation started on September 1st and finished on October 31st 1998.

The RMSE method was used to quantify the reproducibility of the model. This verification exercise indicated that the reproducibility of the model was acceptable in the coastal zone (Figure 10). Results indicate that the modeled profiles were in good agreement with the depth of the observed halocline and salinity values observed in situ. These data suggest that the contribution of the simulated freshwater discharge of the Patos Lagoon and the La Plata River is in accordance with the expected conditions observed along the inner continental shelf during spring. According to Ciotti et al. (1995), coastal waters exhibit thermohaline characteristics that vary with the annual cycle of river runoff and mixing with offshore waters. Soares and Möller (2001) observed salinities of the adjacent coastal waters in the Southern Brazilian Shelf ranging from 24 to 34.5 during spring period. The RMSE analysis indicated good results apart from the complex temporal and spatial variability of shelf dynamics with absolute errors lower than 3.6 (Figure 10). Zero lag correlation analysis was

performed and the results indicated good correlation coefficients greater than 0.87 for all the calculated salinities in daily time scales (Figure 10).

The Kleine and McClintock (1953) formulation was used to estimate the mean uncertainty propagation provided by the numerical model in the potential energy anomaly equation based on the verification tests (table I). The calculated local variation of the potential energy anomaly is of magnitude order around $10^{-4}$ $Wm^{-3}$ in the near field, and $10^{-5}$ $Wm^{-3}$ in the far field. The propagated errors are at least two orders lower than the calculated ones (values < $10^{-6}$ $Wm^{-3}$). The major errors (values between $10^{-6}$ and $10^{-7}$ $Wm^{-3}$) are associated with the straining and to the up- and downwelling processes ($S_x$, $S_y$ and $W_z$ terms) because of the deviations from the depth mean values of velocities and due some uncertainty associated with the prediction of vertical velocities. However, the numerical model can be considered able to predict velocities and density fields to be used in the potential energy anomaly investigations, because there are low RMSE errors, high correlation and no phase lags between calculated and estimated, besides small propagated errors trough the results in daily and longer time scales.

## 5. Results

### 5.1. Temporal variability of the mixing process

In order to investigate the dominant terms controlling the mixing process in the near and far fields of the Patos Lagoon coastal plume, a model simulating the physical parameters established in section 2.3 was carried out for 688 days. The simulated period ranged from January 1$^{st}$ 1998 to November 19$^{th}$ 1999. The Patos

Lagoon coastal plume is a physical system governed by a range of time scales. Therefore, the time scales of each of the main dominant mechanisms controlling the mixing behavior of that plume were investigated separately. The spectral content and the correlation between the potential energy anomaly $\varphi_t$ time series, wind intensity and freshwater discharge were carried out at Points 1, 2 and 3 (see Figure 1C) using cross-wavelet analysis. This method locates power variations within the discrete time series over a range of scales and provides the local and the global power spectrum.

The analysis of the local power spectrum (Figures 11B, 11E, 11H, 12B, 12E and 12H) indicated in general way two main groups of time scales controlling the mixing behavior of the Patos Lagoon coastal plume. In the first group, the physical processes are associated with the local wind influence (periods shorter than 16 days). These processes are responsible for the maintenance of the potential energy anomalies at the Patos Lagoon coastal plume at synoptic time scales. Otherwise, in the second group, the freshwater discharge contributes to these anomalies in a wide range of time scales covering: monthly (20 - 25 days), intra-seasonal to seasonal (64 - 128 days) and almost annual (256 - 344 days) cycles.

Analysis of the local power spectrums (Figure 11B, 11E and 11H) indicate the influence of winds occurring during the whole studied period. Their contribution is most effective to the maintenance of potential energy anomalies in the far field of the plume (point 2) during periods of high freshwater intensity during the 1998 year (from day 1 to day 365) and from autumn to spring of 1999 (after day 500). During periods of low freshwater intensity from summer to autumn of 1999 (from day 365 to day 500), the wind influence is almost restricted to the near field (point 1) of the Patos Lagoon coastal plume. Local power spectrums (Figure 12B, 12E and 12H) indicate

the contribution of freshwater discharge occurring during periods of moderate and high freshwater influence.

The contribution of the monthly, intra-seasonal and seasonal cycles are most effective to the maintenance of anomalies in the near field of the plume (point 1) during periods of high freshwater during the 1998 year and at the end of 1999. In the far field (point 2) the freshwater contribution in these shorter time scales are most restricted because of the less intense freshwater discharge. The longer cycle associated with the annual variability of freshwater discharge in the study region appears remarkable from the winter of 1998 to the winter of 1999 (from day 150 to day 450) and their influence extend from the near to the far field of the plume.

The global power spectrum of the potential energy anomaly $\varphi_t$ time series (Figures 11C, 11F, 11I, 12C, 12F and 12I) corroborate these findings and indicate the importance of these processes in the different regions of the plume highlighting the separate contributions of the local wind influence (periods lower than 16 days) and the direct freshwater input into the inner continental shelf occurring in longer time scales (from 20 to 344 days).

### 5.2. Covariance analysis: plan views of $\varphi_t$ distribution and $\varphi_t$ predictors

The covariance method was used to investigate the spatial variability of the dominant terms that control mixing processes. Covariance between the individual terms (equation 1.4a) and the local variation of the potential energy anomaly ($\varphi_t$) are presented in Figures 13, 14 and 15. Based on the cross wavelet spectrums the

covariance analyses were performed for three important time scales selected as representative of winds and freshwater discharge contributions.

In order to investigate the contribution of winds, a period was selected a period of 685 days with time step of 5 days (Figure 13), and another period of 675 days with time step of 15 days to perform the covariance analysis (Figure 14). The contribution of freshwater discharge was investigated using a period of 660 days with a time step of 30 days to perform the covariance analysis (Figure 15). According to equation 1.5a, the magnitude of the covariance depends on the product of $\varphi_t$ and the term under consideration. Therefore, anomalies in $\varphi_t$ are stronger in regions where the covariance is high (reddish regions), or the term under consideration is important to the maintenance of these anomalies.

The auto-variance ($\varphi^2_t$) presented in Figures 13, 14 and 15 indicates the contribution of all the terms to the potential energy anomaly. The mean position of the 24 and 26 isohalines were calculated and indicate the dominant spreading of the superficial salinity field toward the southwest during the 688 days of simulation. The isohalines indicate the mean position of the frontal region of the plume. The largest $\varphi_t$ variations are restricted to the near field of the plume (near the Patos Lagoon mouth) and at the transition of the frontal region (isohaline of 24). Intermediate values are observed beyond the frontal region, in the far field and further downstream, outside of the plume.

The covariance between SUMT and $\varphi_t$ is very similar to the auto-variance in the inner and far fields of the plume, indicating that the first 9 terms of equation 1.4a are the most important for determining $\varphi_t$ variability of the Patos Lagoon coastal plume (Figures 13, 14 and 15). Auto-variance analyses indicate that mixing processes associated with the local wind action (Figures 13 and 14) are most effective

controlling the potential energy anomalies in the near and far field of the Patos Lagoon coastal plume, while, the anomalies associated with the monthly freshwater discharge variability are most restricted to the near field (Figure 15). The covariance between AS and $\varphi_t$ exhibits a similar behavior, although the lower values observed in the near field indicate the contribution of other processes that are not included in the AS variability. Similar values are observed near the frontal region in the AS and SUMT covariance maps, with differences observed southwestward, further from the plume. This result suggests that, in the far field, the advection and straining terms are representatives to explain the stratification/mixing processes, and the sum of the dispersion, non linear and vertical advection terms largely cancel out. On the other hand, these terms can be important in the near field.

Straining and advection terms seem to be the most important contributions to the potential energy anomalies from few days up monthly time scales. The individual contributions of straining and advection terms are presented in Figures 13, 14 and 15. Cross-shore straining is important in the near field region, suggesting that deviations of the cross shore depth-mean velocity influence considerably the dynamics of this region. The along-shore straining occurring along the entire body of the plume is indicative of the regions with high deviations of depth-mean along-shore component of velocity. The advection due to the vertical mean horizontal velocity seems to be important in the near and far fields, and the dominant transport is in the southwest direction, with moderate spreading as the plume moves offshore.

The terms that describe the non-linear interactions between deviations in density and velocity over the vertical direction (terms $N_x$ and $N_y$), and their depth averaged counterparts (terms $C_x$ and $C_y$) are similar to the advection and straining terms presented above. These results indicate that interactions between deviations in

density and velocity in this region contribute to the stratification (mixing) of the water column modulating the advection and straining effects. These terms present major contribution in shorter times scales (Figures 13 and 14) modulating the straining and advective processes associated with the local wind action in the near and far field. The vertical advection contributes effectively to the stratification evolution in the near field of the Patos Lagoon coastal plume, where an intense vertical component of velocity is observed, in all the time scales.

### 5.3. Covariance analysis: $\varphi_t$ distribution and $\varphi_t$ predictors in the near and far field

In order to investigate the contribution of each of the individual terms in equation 1.4a to the variability in potential energy anomaly ($\varphi_t$) at specific points located in the near and far field of the Patos Lagoon coastal plume, a time series of potential energy anomalies were extracted at three stations (see Figure 1C) and compared with the time series of each individual term by the covariance and correlation parameters for each of the time scales related to the wind action (Tables II and III) and to the freshwater discharge (Table IV).

Point 1 (Figure 1C) is located in the near field, close to the Patos Lagoon mouth. The covariance for the potential energy anomaly time series (PHI) decreases from the shorter (5 days) to the longer (30 days) time scales. A general overview shows that the first nine terms of the equation (SUMT) are responsible for the majority of the potential energy anomaly at this point. The analysis for the other terms of the equation indicate that the most important term is vertical advection ($W_z$) which exhibits high covariance and correlation with the potential energy anomaly $\varphi_t$ time

series in all the different time scales (Tables II, III and IV). This result suggests that the area close to the mouth is dominated by vertical advection effects that generate negative (positive) $\varphi_t$ anomalies and the downward (upward) displacement of isopycnals. The secondary contribution is associated with the along-shore dispersion term ($C_y$) indicating a moderate contribution to the maintenance of the stratification in this region (Tables II, III and IV).

Point 2 (Figure 1C) was located in the frontal region of the Patos Lagoon coastal plume. The covariance of the potential energy anomaly time series (PHI) decreases in the same way as the point 1. In this region, advection and straining terms (AS) appeared to be the most important during the entire simulation period. From the four terms, along-shore straining ($S_y$) and advection ($A_y$) were the most important terms that contributed to the positive anomalies of $\varphi_t$. The cross-shore advection ($A_x$) provided an important contribution to negative anomalies of $\varphi_t$. In this region, the advection effects are still negatively modulated by non linear effects ($N_y$ e $N_x$) providing contributions to the negative anomalies of $\varphi_t$ (Tables II, III and IV).The influence of AS terms were reflected by the enhancement of stratification (mixing) near the frontal region represented by positive (negative) anomalies in $\varphi_t$. Their importance was probably due to the intermittent advection of the less dense waters provided by the Patos Lagoon discharge.

At Point 3 (Figure 1C), the major differences were observed from shorter to longer time scales. In this region, advection and straining terms (AS) appeared to be the most important during the entire simulation period in all the time scales. However, the effects of non linearities and dispersion (Table II and III) are important to perform potential energy anomalies. Across-shore straining (Sx) and advection (Ax) are the most important contribution to the positive anomalies of $\varphi_t$. However, the non

linearities contribute to negative anomalies differently for each of the time scales analyzed (Table II, III and IV). In time scales of 5 days, important contributions of $N_x$ and $N_y$ are observed, and, for semimonthly ones, just the along-shore component ($N_y$) presents some importance. The across-shore component ($N_x$) is significant only for longer time scales associated with the freshwater discharge influence. The along-shore dispersion term ($C_y$) provides some contribution to the positive anomalies in scales associated with the wind influence.

The time series for other points between the 24 and 26 isohalines were also analyzed (not shown). Points located northeastward of the frontal region exhibited similar behavior to Point 3, while the regions located southwestward were similar to Point 2. The results above suggest that, in the near field close to the Patos Lagoon mouth, the vertical advection explains most of $\varphi_t$ variability. On the other hand, the four terms accounting for cross-shore and along-shore straining and advection explain most of $\varphi_t$ variability in the frontal region and far field. The nonlinearities and dispersion terms are not negligible, but their contribution is associated with modulation effects, especially near the frontal region and during periods of high fluvial discharge.

The results summarizing the contribution of the principal straining and advection terms accounting for the potential energy anomaly in the Patos Lagoon coastal plume considering all the time scales are presented in Figure 16. This figure demonstrates the dominant southwestward propagation associated with the mean conditions of the current velocity in the inner shelf during the 688 days of simulation. This result indicates that stratification and mixing process were controlled differently in some regions of the plume. Three specific regions were defined: the region near the Patos Lagoon mouth, dominated by vertical advection ($W_z$ term); the northeast part of

that plume, controlled by the cross-shore straining and advection ($S_x$ and $A_x$ terms); and the region located to the south of the Patos Lagoon mouth, controlled by the along-shore straining and advection ($S_y$ and $A_y$ terms) and cross-shore advection ($A_x$ term).

### 5.4. Time series analysis of the $\varphi_t$ distribution

In order to analyze the contribution of the different physical mechanisms to the maintenance of the potential energy anomaly ($\varphi_t$) near the mouth of Patos Lagoon and the frontal region during typical wind conditions. Time series of $\varphi_t$ as well as the horizontal and vertical advection and straining terms were selected during the whole period 685 days considering time step of 5 days. The most intense anomalies were observed near the Patos Lagoon mouth because of the higher velocities and intense density gradients observed in these regions (Figure 17). In this region (Figure 17A), vertical advection ($W_z$) controlled the $\varphi_t$ anomalies. Near the frontal region (Figure 17B), the along-shore advection and straining effects ($A_y$ and $S_y$) explained the majority of the $\varphi_t$ variability. The influence of the different mechanisms can induce positive or negative anomalies during different wind conditions (Figures 17A and 17B).

In order to accomplish that, the mechanisms controlling the $\varphi_t$ variability were analyzed during two different events (day 220 and 390). During the first event, northwest winds induced the spreading of the plume southwestward (Figure 18A), promoting the stratification of the water column in the far field (Point 2) and the dominant upward velocities close to the mouth of the Patos Lagoon (Point 1) (Figure 18C). These dynamic conditions induced the positive anomalies observed at Point 1

and Point 2 (Figure 17). During the second event, southwest winds induced the spreading of the plume northeastward (Figure 18B), promoted the mixing of the water column in the far field (Point 2) and the dominant downward velocities close to the mouth of the Patos Lagoon (Point 1) (Figure 18D). These dynamic conditions induced the negative anomalies observed at Point 1 and Point 2 (Figure 17).

## 6. Discussion

Previous study of Marques et al. (2009) verified the importance of the freshwater intensity to the formation and maintenance of the Patos lagoon coastal plume, and the importance of the local wind action promoting the stratification and mixing of the coastal waters. In this paper, the contribution of each mechanism controlling the stratification evolution of the adjacent coastal waters and their importance according to different time scales was carried out through numerical modeling.

### 6.1. Dominant cycles controlling stratification and mixing processes

The direct analysis of the potential energy anomaly time series revealed strong variability on several days time scale following the local wind action and the river discharge pattern over the study region. The river discharge influences these anomalies in a wide range of variability from monthly to annual time scales. Monthly modulation is associated with the precipitation during meteorological systems passage. The intra-seasonal, seasonal and annual variability of the meteorological systems passage perform the longer cycles of the Patos Lagoon river discharge, and

the remote effects associated with the oceanic and meteorological circulation variability control these longer cycles.

There are important differences in the power variability observed in the near and far field regions of the plume. In the near field, the power is around one order of magnitude higher than near the frontal region. Close to the Patos Lagoon mouth, the most energetic events occurred intermittently during the entire simulated period, indicating the occurrence of stratification/de-stratification processes associated with the exchange process between the estuarine and coastal region during low or high river discharge events. On the other hand, in the frontal region of the plume, the most energetic events were observed only during moderate and high fluvial discharge periods. These results indicated that far field regions were more influenced by the stratification/de-stratification processes associated with the advection of less dense waters during moderate and high discharge events, as in entire 1998 year and the second half of 1999.

During El Niño years (e.g., 1998), the far field is most influenced by the coastal plume, but the freshwater discharge pattern in southern Brazil can be intensified due to positive precipitation anomalies associated with these climatic events (Grimm et al., 1998; 2000). Normal situations, which occur during the austral summer and fall, in the Southern Brazilian Shelf, usually exhibit low freshwater discharge, contributing for the formation of small coastal plumes and less stratified waters. Some authors verified seasonal patterns of stratification along different coastal sites. van Aken (1986) showed that in certain areas of the North Sea, the initial onset of the seasonal stratification may be caused by differential advection in the presence of a strong horizontal salinity gradient. Rippeth and Simpson (1996) verified that

during transition from spring to summer, the region of Clyde Sea became susceptible to complete vertical mixing episodes due to an inversion of the temperature structure.

The power variation analysis indicated that events occurring in periods shorter than 20 days associated with the local wind influence were the main mechanism that controlled the potential energy anomaly in the Patos Lagoon coastal plume. The local wind influence is principally associated with the direct momentum transference to the water column. On the other hand, the direct river discharge effects in 30 days cycles were restricted controlling the potential energy anomalies in the near field of the plume. The river discharge influence is associated with the inertia of the flux introduced in the adjacent region.

Several studies using time series analysis and numerical simulations showed that mixing and exchange processes during low and mean discharge conditions of the Patos lagoon circulation pattern were controlled by wind effects at synoptic times scales that were coincident with the passage of meteorological systems every 3 to 17 days (Möller, 1996; Möller et al., 1996; Möller et al., 2001; Fernandes, 2001; Fernandes et al., 2002; Fernandes et al., 2004; Fernandes et al., 2005; Castelão and Möller, 2006, Marques et al. (submitted)). Marques et al. (2009) observed a similar pattern of migration southwestward/northeastward of the Patos Lagoon coastal plume according with the passage of meteorological systems over the area.

The Patos Lagoon coastal plume is a medium scale plume dominated by the wind action (Marques et al. 2009). The coastal plume develops mainly in a region where stratification can change abruptly. The velocities in the lower half of the water column tend to de-stabilize the water column. Velocity conditions like this are observed in this region during the occurrence of winds that favor upwelling (north quadrant winds), resulting in the dispersion of brackish waters southwestward and

promoting stratified and stable profiles. Burrage et al. (2008) investigated the interaction of the Patos Lagoon coastal plume and the La Plata River plume by contrasting winter (2003) and summer (2005) conditions. These authors verified that the La Plata plume is highly asymmetric, with alongshore development towards the north and a dynamic behavior that is similar to a buoyant coastal boundary current in which the geostrophic across-shelf momentum is nearly balanced.

The Patos Lagoon coastal plume, on the other hand, maintained its integrity as a relatively symmetric, ageostrophic, frictionally dominated plume with significant across-shelf and modest along-shelf development. Marques et al. (2009) verified through EOF analysis that the principal mode of variability of the Patos Lagoon coastal plume (explaining 70% of the variability), indicating the southwestward plume transportation, is controlled by the combination between the dominant north quadrant winds (upwelling favorable winds) and seasonal fluvial discharge variability over the study region. These authors verified that the second mode, which was associated with the passage of frontal systems, was responsible for the intermittent migration of the plume northeastward and enhancement of mixing process.

None of these studies, however, investigated the contribution of each mechanism that controls the mixing of the adjacent coastal waters, and in particular, the effects of straining and advection on the stratification/de-stratification process along the Southern Brazilian inner shelf. However, the analyses presented in this paper corroborate the results obtained by Marques et al. (2009) confirming that north quadrant winds induce upward velocities in the near field and enhance the advection of freshwater southwestward. These dynamic conditions increase the stratification and the potential energy anomalies along the adjacent coastal region. Otherwise, south quadrant winds promote the advection of the Patos Lagoon coastal plume

northeastward promoting downward velocities in the near field. In these conditions the mixing processes are intensified and negative potential energy anomalies are observed.

### 6.2. Evolution of stratification and mixing processes

The potential energy anomaly equation has been used in several studies to quantify the contribution of different mechanisms that promote the mixing of stratified systems in estuaries and coastal seas (van Aken, 1986; Sharples and Simpson, 1993; Rippeth and Simpson, 1995; Simpson et al., 2002; Burchard and Hofmeister, 2008; de Boer et al., 2008; among others). In this study, the potential energy anomaly equation performed sufficiently for investigating the dominant terms controlling the stratification along the Southern Brazilian inner shelf region influenced by the Patos Lagoon coastal plume. The analysis considered 688 days of simulation and indicated that the advection and straining terms accounted for almost all the variability of the stratification and mixing process considering the local wind influence (cycles of 5 and 15 days) and the direct river discharge influence (cycle of 30 days).

Non-linear interactions between deviations in both density and velocity over the vertical direction, as well as the dispersion terms, were important everywhere, but were associated with modulation effects. The non-linear terms and along shore dispersion are the most important modulators associated with the wind and river discharge variability in the near and far field. This behavior indicates that deviations in direction and intensity of wind or currents, occurring form one day to the other, are transferred to the water column inducing deviations. The importance of along shore

dispersion term suggests that most important deviations are occurring in the along shore wind or current components. The across-shore non linear term is the most important modulator effect associated with the discharge monthly cycles because of the orientation of jetties that promotes southeast ebb currents.

Different regions of the plume exhibit contrasting regimes that were spatially distributed with different balances of terms. de Boer et al. (2008) investigated the plume in the Rhine region, and Burchard and Hofmeister (2008) analyzed numerical results of a two-dimensional idealized estuary and observed a similar pattern, with advection and straining controlling the evolution of stratification and de-stratification conditions. They also observed different balances of terms at different positions. In the near field, close to the Patos Lagoon mouth, vertical advection controls the stratification and mixing processes. In this region, the strongest velocities were observed due to gravitational circulation and the choking of the jetties. Topographic characteristics of the seaward part of the channel favored the intensification of the vertical circulation. In this region of stable stratification, downward velocities generated downward displacement of the isopycnals in the water column, decreasing the potential energy anomalies, and vice versa.

According to Hetland (2005) the vertical mixing and corresponding entrainment of background waters was greatest near the estuary mouth, where inertial shear mixing was large. The very near field of the plume was characterized by rapid acceleration and strong shoaling, and the presence of turbulence decelerated the advancement of the plume, modifying the rate of width expansion (Macdonald et al., 2007). Burchard and Hofmeister (2008) found that the strongest contribution of the vertical advection was close to the head of the estuary, where shoaling of the isohalines was observed. The results presented by de Boer et al. (2008) indicated that

the region close to the river mouth was the most affected by non-linear interactions and vertical advection.

The four terms accounting for cross-shore and along-shore straining and advection explained most of potential energy anomaly budget in the frontal region and far field of the Patos Lagoon coastal plume. Therefore, two regions with different contributions of these terms were considered. The northeast part of the plume was characterized by the convergence between the coastal currents and ebb flows associated with the Patos Lagoon freshwater discharge. This condition promoted the maximum spreading of the plume offshore and the domination of the cross-shore straining and advection terms that controlled the stratification and mixing process. The southwest part of the plume was dominated by the coastal currents, creating the maximum spreading of the plume alongshore and the dominance of upwelling processes. These conditions corroborated the observation that the alongshore straining, advection and cross-shore advection terms controlled the evolution of stratification in this region. The simultaneous occurrence of moderate or high discharge events and southwestward (northwestward) currents contributed to the spreading of freshwater along-shore, stratifying (mixing) the water column and increasing (decreasing) the potential energy anomaly.

According to the dominant physical process and the time scales considered, different regions exhibited distinct mechanisms that controlled the evolution of stratification were commonly observed. According to Hetland (2005), plumes can be divided into two dynamically distinct regions: the near field, characterized by both inertial shear mixing and wind mixing, and the far field, characterized by only wind mixing, if present. Mixing within the plume, caused by advective shear mixing and wind stress, is related to the surface area of the isohalines within the plume (Hetland,

2005). The dominance of upwelling favorable winds in the study region resulted in a mean transport that was southwestward of the Patos Lagoon coastal plume during the 688 days of simulation. Previous studies demonstrated that the plume became thinner and was advected offshore by the cross-shore Ekman transport that was induced by upwelling favorable winds (Chao, 1988b; Kourafalou, 1996a, 1996b; Fong and Geyer, 2001; Soares et al., 2007b; Xia et al., 2007, Marques et al., 2009). Soares et al. (2007b) and Marques et al. (2009) observed that upwelling favorable winds initially caused an increase of the vertical stratification due the offshore removal of the riverine waters. Fong and Geyer (2001) and Soares et al. (2007b) verified that thin plumes show stronger vertical velocity shear in the front of the plume, promoting intense mixing and downward entrainment of the plume water, thus reducing stratification.

## 7. Conclusions

The importance of the physical mechanisms controlling the stratification and de-stratification processes along the Southern Brazilian inner shelf that is influenced by the Patos Lagoon coastal plume was investigated through numerical modeling experiments and the application of the potential energy anomaly equation. Results from 688 days of simulation indicated that straining and advection terms were the most important mechanisms for the maintenance of the stratification of the adjacent coastal region accounting for processes associated with the local wind action (cycles of 5 and 15 days) e river discharge input (cycles of 30 days). Nonlinearities and dispersion terms were important for modulation effects during periods of high fluvial discharge. The main conclusions of this study were as follows:

- Analysis of the potential energy anomaly time series revealed strong variability that occurred within several days and followed the wind pattern over the study region. This variability was accompanied by the monthly modulation of river discharge and remote effects associated with variability in oceanic circulation.

- Close to the Patos Lagoon mouth the occurrence of stratification/de-stratification processes are associated with the exchange process independently of the river discharge intensity. In the frontal region and far field, these processes were more influenced by the advection of less dense waters.

- Considering the mean conditions, the Patos Lagoon coastal plume advanced southwestward, resulting from dominant upwelling favorable winds. This resulted in the maximum spreading of the plume along-shore, with moderate offshore transportation and a stratified and stable water column.

- Close to the mouth of the Patos Lagoon, vertical advection explained most of the evolution of stratification. In this region, stronger velocities, which resulted from gravitational circulation and their interaction with topographic characteristics of the sea bed, contributed to the intensification of the vertical circulation.

- The northeast part of the plume (frontal region) was characterized by the convergence between the coastal currents and ebb flows associated with the freshwater discharge. This condition promoted the dominance by the cross-shore straining and advection terms, which enhanced the maximum spreading of the plume offshore.

- The southwest part (far field) was controlled by the coastal currents, resulting in the dominance by the alongshore straining and advection and cross-shore advection terms. This condition enhanced upwelling and the spreading of the plume alongshore.

- Close to the mouth of the Patos Lagoon, the occurrence of downward velocities generated downward displacement of the isopycnals in the water column, decreasing the potential energy anomalies, and vice versa.

- During moderate to high discharge events (near the frontal region and far field): the northeastward currents induce the advection of the plume northeastward intensifying the mixing processes and decreasing the potential energy anomalies. On the other hand, the southwestward currents intensified the spreading of freshwater, increasing the stratification and the potential energy anomalies.

This paper inserts some implications relating a novel method to analyze potential energy anomaly through the wavelets. One important finding is the multiples scales controlling the stratification evolution of the Patos lagoon coastal plume. A suggestion for further research should carry out studies considering the two principal groups of time scales observed in this paper with idealized simulations: a simple wind case and a simple fluvial discharge event case. Other important point should be investigated in the future research is related to the importance of different time scales for stratification evolution of the Patos Lagoon coastal plume considering processes

with periods lower than one day, influenced by astronomical tides, as well as, the processes longer than one year, associated with El Niño events.

## 8. Acknowledgments

The authors are grateful to the *Conselho Nacional de Pesquisa e Desenvolvimento (CNPq)* for sponsoring this research under contracts: 590006/2005-3, 476696/2007-0 and 308796/2008-0. Further acknowledgements go to the Brazilian Navy for providing detailed bathymetric data for the coastal area, to the Brazilian National Water Agency (ANA) and the National Oceanic & Atmospheric Administration (NOAA) for supplying the fluvial discharge and wind data sets, respectively, and to the HR Wallingford for providing the academic license of the TELEMAC System to accomplish this research.

## 9. References

Burchard, H., Hofmeister, R., 2008. A dynamic equation for the potential energy anomaly for analyzing mixing and stratification in estuaries and coastal seas. Estuarine, Coastal and Shelf Science 77(2008), 679-687.

Burrage, D., Wesson, J., Martinez, C., Pérez, T., Möller Jr, O., Piola, A. 2008. Patos Lagoon outflow within the Rı´o de la Plata plume using an airborne salinity mapper: Observing an embedded plume. Continental Shelf Research. 28(2008), 1625-1638.

Castelão, R. M., Möller, O. O., 2006. A modeling study of Patos Lagoon (Brazil) flow response to idealized Wind and river discharge: Dynamical analysis. Brazilian Journal of Oceanography. 54(1), 1-17.

Castro, B., Miranda, L. B., 1998. Physical Oceanography of the western Atlantic continental shelf between 4°N and 34°S. In: Brink, K. and Robinson, A. (Eds.), The Sea – The Global Coastal Oceans, John Wiley & Sons, Inc. Vol. 10, chapter 8, pp. 209-251.

Ciotti, A. M., Odebrecht, C., Fillmann, G., Möller, O. O., 1995. Freshwater outflow and subtropical convergence influence on phytoplankton biomass on the southern Brazilian continental shelf. Continental Shelf Research. 15(14), 1737-1756.

Chao. S-Y., Boicourt, W.C., 1986. Onset of estuarine plumes. Journal of Physical Oceanography. 16, 2137-2149.

Chao, S-Y., 1988a. River-Forced estuarine plumes. Journal of Physical Oceanography. 18, 72-88.

Chao, S.-Y., 1988b. Wind-driven motion of Estuarine plumes. Journal of Physical Oceanography. 18, 1144-1166.

Chapman, D. C., Lentz, S. T., 1993. Trapping of a coastal density front by the bottom boundary layer. Journal of Physical Oceanography. 24, 1464-1479.

de Boer, G. J., Pietrzak, J. D., Winterwerp, J. C., 2008. Using the potential energy anomaly equation to investigate tidal straining and advection of stratification in a region of freshwater influence. Ocean Modeling 22(2008), 1-11.

Fernandes, E. H. L., 2001. Modelling the hydrodynamics of the Patos Lagoon, Brazil. DSc. Thesis, Institute of Marine Studies Faculty of Science, University of Plymouth, England.

Fernandes, E. H. L., Dyer, K. R., Möller, O. O., Niencheski, L. F. H., 2002. The Patos Lagoon hydrodynamics during an El Niño event (1998). Continental Shelf Research 22(2002):1699-1713.

Fernandes, E. H. L., Mariño-Tapia, I., Dyer, K. R., Möller, O. O. 2004. The attenuation of tidal and subtidal oscillations in the Patos Lagoon estuary. Ocean Dynamics. 54, 348-359.

Fernandes, E. H. L., Dyer, K. R., Möller, O. O., 2005. Spatial gradients in the flow of Southern Patos Lagoon. Journal of Coastal Research. 20, 102-112.

Flather, R. A., 1976. Results from surge prediction model of the North-West European continental shelf for April, November and December1973. Institute of Oceanography (UK), Report nº 24.

Fong, D. A., Geyer, W. R., 2001. Response of a river plume during an upwelling favorable wind event. Journal of Geophysical Research. 106(C1), 1067-1084.

Fong, D. A., Geyer, W. R., 2002. The Alongshore transport of freshwater in a surface-trapped river plume. Journal of Physical Oceanography. 32, 957-972.

Framiñan, M. B., Brown, O. B., 1996. Study of the La Plata turbity front, Part I: spatial and temporal distribution. Continental Shelf Research. 16(10), 1259-1282.

Grimm, A. M., Ferraz, S. E. T., Julio, G., 1998. Precipitation anomalies in southern Brazil associated with El Niño and La Niña events. American Meteorological Society. 11, 2863-2879.

Grimm, A. M., Barros, V. R., Doyle, M. E., 2000. Climate variability in southern South America associated with El Niño and La Niña events. American Meteorological Society. 13(1), 35-58.

Guerrero, R. A., Acha, E. M., Framiñan, M. B., Lasta, C. A., 1997. Physical oceanography of the Rio de La Plata estuary, Argentina. Continental Shelf Research. 17(7), 727-742.

Guo, X., Valle-Levinson, A., 2007. Tidal effects on estuarine circulation and outflow plume in the Chesapeake Bay. Continental Shelf Research. 27(2007), 20-42.

Hervouet, J-M., 2007. Free surface flows: Modelling with the finite element methods. John Wiley & Sons Ltd, Copyright © 2007, England.

Hetland, R. D., 2005. Relating River Plume structure to vertical mixing. Journal of Physical Oceanography. 35, 1667-1688.

Kleine, S., McClintock, F. 1953. Describing uncertainties in single sample experiments. Mechanical Engineering, 75. pp3.

Kourafalou, V. H., Oey, L. Y., Wang, J. D., Lee, T. N., 1996a. The fate of river discharge on the continental shelf 1: Modeling the river plume and the inner shelf coastal current. Journal of Geophysical Research. 101(C2), 3415-3434.

Kourafalou, V. H., Lee, T. N., Oey, L. Y., Wang, J. D. 1996b. The fate of river discharge on the continental shelf 2: Transport of coastal low-salinity waters under realistic wind and tidal forcing. Journal of Geophysical Research. 101(C2), 3435-3455.

MacDonald, D. G., Goodman, L., Hetland, R. D., 2007. Turbulent dissipation in a near-field river plume: A comparison of control volume and microstructure observations with a numerical model. Journal of Geophysical Research 112(C07026), doi:10.1029/2006JC004075.

Mann, K. H. and Lazier, J. R. N., 1991. Dynamics of marine ecosystems: Biological-Physical interactions in the Oceans. In: Blackwell Scientific Publications, Inc, Boston.

Marques, W. C., 2005. Padrões de variabilidade temporal nas forçantes da circulação e seus efeitos na dinâmica da Lagoa dos Patos, Brasil. MSc Thesis, University of Rio Grande, Rio Grande do Sul, Brasil, unpublished.

Marques, W. C., Fernandes, E. H., Monteiro, I. O., Möller, O. O., 2009. Numerical modeling of the Patos Lagoon coastal plume, Brazil. Continental Shelf Research 29(2009), 556-571.

Marques, W. C., Möller, O. O., 2009. Variabilidade temporal em longo período da descarga fluvial e níveis de água da Lagoa dos Patos, Rio Grande do Sul, Brasil. Revista Brasileira de Recursos Hídricos 13, 155-163.

Marques, W. C., Monteiro, I. O., Möller, O. O., (*submitted*). The Exchange processes in

the Patos Lagoon estuarine channel, Brazil. Estuaries and Coasts.

Möller, O. O., 1996. Hydrodinamique de La Lagune dos Patos, Mésures et Modelisation. DSc. Thesis, Université Bordeaux I, France.

Möller, O. O., Lorenzzetti, J. A., Stech, J. L., Mata, M. M., 1996. The Patos Lagoon summertime circulation and dynamics. Coastal Shelf Research. 16, 335-351.

Möller, O. O., Castaing, P., Salomon, J. C., Lazure, P. 2001. The influence of local and non-local forcing effects on the subtidal circulation of Patos Lagoon. Estuarios. 24, 297-311.

Morey, S. L., Martin, P. J., O'Brien, J. J., Wallcraft, A. A., Zavala-Hidalgo, J., 2003. Export pathways for river discharged fresh water in the northern Gulf of Mexico. Journal of Geophysical Research. 108(C10), 3303-3318.

O'Donnel, J., Garvine, R. W., 1983. A time dependent, two layer frontal model of buoyant plume dynamics. Tellus. 35, 73-80.

O’Donnel, J., 1990. The formation and fate of a river plume: A numerical model. Journal of Physical Oceanography. 20, 551-569.

Piola, A. R., Matano, R. P., Palma, E. D., Möller, O. O., Campos, E. J. D., 2005. The influence of the Plata River discharge on the western South Atlantic shelf. Geophysical Research Letters. 32, doi:10.1029/2004GL021638.

Rabalais, N., N., Turner, R., E., Justic, D., Dortch, Q., Wiseman, W. J., 1999. Characterization of hypoxia: Topic 1 report for the Integrated Assessment on Hypoxia in the Gulf of Mexico. NOAA Coastal Ocean Program Decision Analysis Series 15, 167pp.

Rippeth, T. P., Simpson, J. H., 1996. The frequency and duration of episodes of complete vertical mixing in the Clyde Sea. Continental Shelf Research 16(7), 933-947.

Rodi, W., 1984. Turbulence models and their applications in hydraulics. A state of the art review. Edition AIRH.

Royer, L., Emery, W. J., 1985. Computer simulations of the Fraser River plume. Journal of Marine Research. 43, 289-306.

Ruti, P. M., Marullo, S., D’Ortenzio, F., Tremant, M., 2008. Comparison of analyzed and measured wind speeds in the perspective of oceanic simulations over the Mediterranean basin: Analyses, QuickSCAT and buoy data. Continental Shelf Research 70(2008), 33-48.

Sharples, J., Simpson, J. H., 1993. Semi-diurnal and longer stability cycles in the Liverpool Bay region of freshwater influence. Continental Shelf Research 15(2/3), 295-313.

Simpson, J. H., Brown, J., Matthews, J., Allen, G., 1990. Tidal straining density currents, and straining in the control of estuarine stratification. Estuaries 13(2), 125-132.

Simpson, J. H., Burchard, H., Fisher, N. R., Rippeth, T. P., 2002. The semi-diurnal cycle of dissipation in a ROFI: model-measurement comparisons. Continental Shelf Research 22(2002), 1615-1628.

Simionato, C. G., Meccia, V. L., Dragani, W. C., Nuñez, M. N., 2006a. On the use of the NCEP/NCAR surface winds for modeling barotropic circulation in the Rio de La Plata estuary. Estuarine, Coastal and Shelf Science. 70(2006), 195-206.

Smagorinski, J., 1963. General circulation experiments with the primitive equation, I. The basic experiment. Weather Review. 91, 99-164.

Soares, I. D., Möller, O. O., 2001. Low-frequency currents and water mass spatial distribution on the Southern Brazilian Shelf. Continental Shelf Research 21(16-17), 1785-1814.

Soares, I. D., Kourafalou, V., Lee, T. N., 2007a. Circulation on the western South Atlantic continental shelf. Part 1: Numerical process studies on Buoyancy. Journal of Geophysical Research. 112, C04002. doi:10.1029/2006JC003618,2007.

Soares, I. D., Kourafalou, V., Lee, T. N., 2007b. Circulation on the western South Atlantic continental shelf. Part 2: Spring and autumn realistic simulations. Journal of Geophysical Research. 112, C04003. doi:10.1029/2006JC003620,2007.

Sutherland, J., 2001. COSMOS modeling and the development of model performance statistics, TR121-EC MAST Project nº MAS3-CT97-0086, HR Wallingford, UK.

Torrence, C., Compo, G. P., 1997. A practical guide to wavelet analysis. Bulletin of the American Meteorological Society.

van Aken, K. M., 1986. The onset of seasonal stratification in shelf seas due to differential advection in the presence of a salinity gradient. Continental Shelf Research 5(4), 475-485.

Zavialov, P. O., Kostinoy, A. G., Möller, O. O., 2003. Mapping river discharge effects on Southern Brazilian shelf. Geophysical Research Letters. 30(21), 2126

Wang, H., Yang, Z., Li, Y., Guo, Z., Sun, X., Wang, Y., 2007. Dispersal pattern of suspended sediment in the shear frontal zone off the Huanghe (Yellow River) mouth. Continental Shelf Research. 27(2007), 854-871.

Wong, K. C., Münchow, A., 1995. Buoyancy forced interaction between estuary and inner shelf observation. Continental Shelf Research 15(1), 59-88.

Wright, I. D., Nittrouer, C. A., 1995. Dispersal of river sediments in coastal seas: six contrasting cases. Estuaries. 18, 494-508.

Wright, L. D., Friedrichs, C. T., 2006. Gravity-driven sediment transport on continental shelves: A status report. Continental Shelf Research. 26(2006), 2092-2107.

Xia, M., Xie, L., Pietrafesa, L. J., 2007. Modeling of the Cape Fear River estuary plume. Estuaries and Coasts. 30(4), 698-709.

Figure 1: The Southern Brazilian Shelf (dotted rectangle), the Patos Lagoon and its principal tributaries (A). The finite elements mesh highlighting the liquid and surface boundaries (B) and the lower Patos Lagoon estuary and adjacent coastal area (C). The location of salinity and temperature profiles (T1,T2), low frequency water levels (L1,L2) and current velocity (V1,V2) used as boundary conditions, as well as, the location of Patos Lagoon estuary and adjacent coastal area (dotted rectangle) are presented in figure 1B. Eight points (S1-S8) of salinity measurements, two of current velocity measurements (MV1, MV2) and three points (P1, P2 and P3) used in the potential energy anomaly analyzes are also presented in Figure 1C.

Figure 2: Surface salinity (A) and temperature (B) fields from January 1998.

Figure 3: Time series of river discharge for the Guaíba (Jacuí + Taquari) and Camaquã rivers from January 1$^{st}$ 1998 to November 18$^{th}$ 1999.

Figure 4: Dominant wind conditions observed in the area. North quadrant (A) and south quadrant (B).

Figure 5: Low frequency water levels (A) and intensity of current velocity (B) prescribed as boundary conditions at the surface layer in two different points along the oceanic boundary of the model.

Figure 6: Low frequency salinity (A) and temperature (B) time series prescribed as boundary conditions at the surface layer in two different points along the oceanic boundary.

Figure 7: Observed and calculated velocity (north/south component) time series at 3 m (A) and 14 m (B) depth at the Praticagem Station between August 2nd and September 22nd 2008. Black dashed line (grey solid line) represents the calculated (observed) time series. The position of these time series MV1 is presented in Figure 1C.

Figure 8: Observed and calculated surface velocity time series at 2 m, component north/south (A) and component east/west (B). Observed and calculated bottom velocity time series at 22 m depth, component north/south (C) and component east/west (D) near the coastal region between August 2nd and September 22nd 2008. Black dashed line (grey solid line) represents the calculated (observed) time series. The position of these time series MV2 is presented in Figure 1C.

Figure 9: Lagged correlation between measurements and modeled results of the current velocity at the Praticagem station (A), and at the coastal area (B).

Figure 10: Salinity profiles from October 26th 1998 in position 1 (A), position 2 (B), position 3 (C), position 4 (D), position 5 (E), position 6 (F), position 7 (G), position 8 (H). The positions of these profiles S1 – S8 are presented in Figure 1C.

Figure 11: Time series of potential energy anomaly $\varphi_t$ at Point 1 (normalized to the maximum value of $\varphi_t$ = 7.14x10$^{-4}$ Wm-³) and wind intensity used for the cross-wavelet analysis (A), as well as the local wavelet power spectrum of the time series using Morlet wavelet (B). Thick contour lines enclose regions of greater than 95%

confidence for a red-noise process with a lag-1 coefficient of 0.72. Cross-hatched regions indicate the cone of influence where edge effects become important. The global wavelet power spectrum (C) of the time series and the dotted line indicate the 95% confidence level. Time series of $\varphi_t$ at station 2 (normalized to the maximum value of $\varphi_t$ = 3.12x10$^{-5}$ Wm-³) and wind intensity used for the cross-wavelet analysis (D), the local wavelet power spectrum of the time series (E) using Morlet wavelet. Thick contour lines enclose regions of greater than 95% confidence for a red-noise process with a lag-1 coefficient of 0.72. Cross-hatched regions indicate the cone of influence where edge effects become important. The global wavelet power spectrum (F) of the time series and the dotted line indicate the 95% confidence level. Time series of $\varphi_t$ at station 3 (normalized to the maximum value of $\varphi_t$ = 9.37x10$^{-6}$ Wm-³) and wind intensity used for the cross-wavelet analysis (G), the local wavelet power spectrum of the time series (H) using Morlet wavelet. Thick contour lines enclose regions of greater than 95% confidence for a red-noise process with a lag-1 coefficient of 0.72. Cross-hatched regions indicate the cone of influence where edge effects become important. The global wavelet power spectrum (I) of the time series and the dotted line indicate the 95% confidence level.

Figure 12: Time series of potential energy anomaly $\varphi_t$ at Point 1 (normalized to the maximum value of $\varphi_t$ = 7.14x10$^{-4}$ Wm-³) and fluvial discharge used for the cross-wavelet analysis (A), as well as the local wavelet power spectrum of the time series using Mexican Hat wavelet (B). Thick contour lines enclose regions of greater than 95% confidence for a red-noise process with a lag-1 coefficient of 0.25. Cross-hatched regions indicate the cone of influence where edge effects become important.

The global wavelet power spectrum (C) of the time series and the dotted line indicate the 95% confidence level. Time series of $\varphi_t$ at station 2 (normalized to the maximum value of $\varphi_t$ = $3.12x10^{-5}$ Wm-³) and fluvial discharge used for the cross-wavelet analysis (D), the local wavelet power spectrum of the time series (E) using Mexican Hat wavelet. Thick contour lines enclose regions of greater than 95% confidence for a red-noise process with a lag-1 coefficient of 0.25. Cross-hatched regions indicate the cone of influence where edge effects become important. The global wavelet power spectrum (F) of the time series and the dotted line indicate the 95% confidence level. Time series of $\varphi_t$ at station 3 (normalized to the maximum value of $\varphi_t$ = $9.37x10^{-6}$ Wm-³) and fluvial discharge used for the cross-wavelet analysis (G), the local wavelet power spectrum of the time series (H) using Mexican Hat wavelet. Thick contour lines enclose regions of greater than 95% confidence for a red-noise process with a lag-1 coefficient of 0.25. Cross-hatched regions indicate the cone of influence where edge effects become important. The global wavelet power spectrum (I) of the time series and the dotted line indicate the 95% confidence level.

Figure 13: The covariance between the various terms in equation 1.4a and $\varphi_t$ as calculated from equation 1.5a. Auto-variance of $\varphi_t$ is proportional to the squared amplitude (A), SUMT indicates the sum of the first nine terms in equation 1.4a(B) and AS indicates the sum of the first four terms in equation 1.4a (C). The color scale is presented in base 2 logarithmic scale in order to improve the visualization. The grey lines indicate the time averaged 24 and 26 isohalines at the surface (averaged over 688 days). Time scale of 685 days with 5 days time step is used in analyzes.

Figure 14: The covariance between the various terms in equation 1.4a and $\varphi_t$ as calculated from equation 1.5a. Auto-variance of $\varphi_t$ is proportional to the squared amplitude (A), SUMT indicates the sum of the first nine terms in equation 1.4a (B) and AS indicates the sum of the first four terms in equation 1.4a (C). The color scale is presented in base 2 logarithmic scale in order to improve the visualization. The grey lines indicate the time averaged 24 and 26 isohalines at the surface (averaged over 688 days). Time scale of 675 days with 15 days time step is used in analyzes.

Figure 15: The covariance between the various terms in equation 1.4a and $\varphi_t$ as calculated from equation 1.5a. Auto-variance of $\varphi_t$ is proportional to the squared amplitude (A), SUMT indicates the sum of the first nine terms in equation 1.4a (B) and AS indicates the sum of the first four terms in equation 1.4a (C). The color scale is presented in base 2 logarithmic scale in order to improve the visualization. The grey lines indicate the time averaged 24 and 26 isohalines at the surface (averaged over 688 days). Time scale of 660 days with 30 days time step is used in analyzes.

Figure 16: Sketch summarizing the dominant terms controlling stratification and mixing process of the Patos Lagoon coastal plume considering process with time scales from 5 to 30 days.

Figure 17: Time series of $\varphi_t$ and the advection and straining terms of equation 1.4a at Point 1 (A), and Point 2 (B) for 685 days. Values were normalized in order to improve visualization.

Figure 18: Salinity in the surface layer of the model for days: 220 (A) and 390 (B). Vertical profiles of salinity and velocity for days 220 (C) and 390 (D). The black line indicates the position of the vertical profile.

Table II. Covariance and correlation parameters between each of the individual terms of equation 1.4 and the potential energy anomaly (PHI) time series at the three points considering processes with periods of 5 days.

| | **Point 1** | **Point 1** | **Point2** | **Point 2** | **Point 3** | **Point 3** |
|---|---|---|---|---|---|---|
| **Term** | **Covariance** | **Correlation** | **Covariance** | **Correlation** | **Covariance** | **Correlation** |
| **PHI** | +5.698 | +100 | +0.267 | +100 | +0.736 | +100 |
| **SUMT** | +5.697 | +99 | +0.266 | +99 | +0.735 | +99 |
| **AS** | -0.092 | -06 | +0.338 | +95 | +0.534 | +62 |
| **$S_x$** | -0.427 | -32 | -0.040 | -75 | +0.088 | +27 |
| **$S_y$** | -0.068 | -43 | +0.164 | +88 | +0.104 | +18 |
| **$A_x$** | +0.560 | +53 | -0.176 | -75 | +0.400 | +23 |
| **$A_y$** | -0.156 | -36 | +0.390 | +90 | -0.059 | -03 |
| **$N_x$** | +0.491 | +33 | +0.068 | +81 | -0.091 | -25 |
| **$N_y$** | +0.121 | +32 | -0.212 | -86 | -0.108 | -16 |
| **$C_x$** | +0.040 | +17 | -0.033 | -31 | -0.071 | -08 |
| **$C_y$** | +0.860 | +77 | +0.115 | +66 | +0.448 | +45 |
| **$W_z$** | +4.275 | +97 | -0.010 | -66 | +0.022 | +31 |

Table III. Covariance and correlation parameters between each of the individual terms of equation 1.4 and the potential energy anomaly (PHI) time series at the three points considering processes with periods of 15 days.

| | **Point 1** | **Point 1** | **Point2** | **Point 2** | **Point 3** | **Point 3** |
|---|---|---|---|---|---|---|
| **Term** | **Covariance** | **Correlation** | **Covariance** | **Correlation** | **Covariance** | **Correlation** |
| **PHI** | +5.559 | +100 | +0.203 | +100 | +0.546 | +100 |
| **SUMT** | +5.558 | +99 | +0.202 | +99 | +0.545 | +99 |
| **AS** | -0.137 | -14 | +0.242 | +94 | +0.570 | +89 |
| **$S_x$** | -0.310 | -31 | -0.020 | -57 | +0.105 | +44 |
| **$S_y$** | -0.057 | -40 | +0.103 | +87 | +0.126 | +33 |
| **$A_x$** | +0.320 | +44 | -0.105 | -59 | +0.274 | +23 |
| **$A_y$** | -0.090 | -28 | +0.265 | +85 | +0.064 | +05 |
| **$N_x$** | +0.352 | +31 | +0.045 | +67 | -0.109 | -40 |

| | | | | | | |
|---|---|---|---|---|---|---|
| **$N_y$** | +0.098 | +29 | -0.135 | -82 | -0.127 | -30 |
| **$C_x$** | +0.054 | +33 | -0.008 | -15 | -0.076 | -18 |
| **$C_y$** | +0.855 | +74 | +0.065 | +61 | +0.277 | +50 |
| **$W_z$** | +4.335 | +97 | -0.007 | -60 | +0.010 | +25 |

Table IV. Covariance and correlation parameters between each of the individual terms of equation 1.4 and the potential energy anomaly (PHI) time series at the three points considering processes with periods of 30 days.

| | **Point 1** | **Point 1** | **Point2** | **Point 2** | **Point 3** | **Point 3** |
|---|---|---|---|---|---|---|
| **Term** | **Covariance** | **Correlation** | **Covariance** | **Correlation** | **Covariance** | **Correlation** |
| **PHI** | +5.276 | +100 | +0.164 | +100 | +0.571 | +100 |
| **SUMT** | +5.275 | +99 | +0.162 | +99 | +0.570 | +99 |
| **AS** | +0.045 | +05 | +0.214 | +95 | +0.602 | +93 |
| **$S_x$** | -0.034 | -03 | -0.034 | -81 | +0.193 | +67 |
| **$S_y$** | -0.066 | -49 | +0.113 | +91 | +0.036 | +09 |
| **$A_x$** | +0.193 | +32 | -0.169 | -80 | +0.662 | +47 |
| **$A_y$** | -0.045 | -16 | +0.305 | +91 | -0.289 | -24 |
| **$N_x$** | +0.024 | +02 | +0.067 | +84 | -0.215 | -64 |
| **$N_y$** | +0.013 | +44 | -0.160 | -89 | -0.021 | -05 |
| **$C_x$** | +0.078 | +45 | -0.035 | -62 | -0.033 | +09 |
| **$C_y$** | +0.820 | +69 | +0.085 | +75 | +0.162 | +30 |
| **$W_z$** | +4.170 | +96 | -0.009 | -68 | +0.009 | +23 |

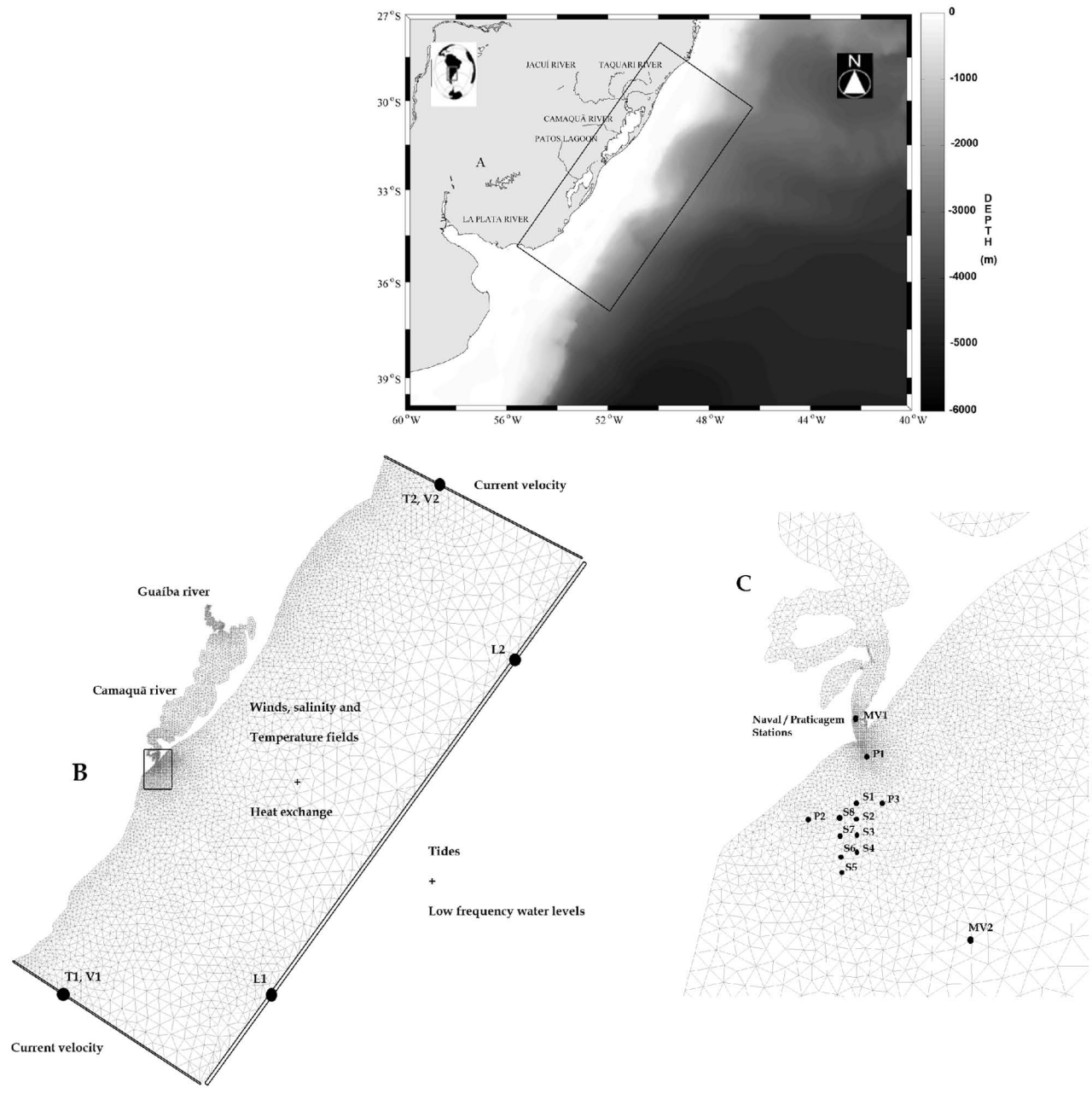
27°S
30°S
33°S
36°S
39°S
60°W
56°W
52°W
48°W
44°W
40°W
JACUÍ RIVER
TAQUARI RIVER
CAMAQUÃ RIVER
PATOS LAGOON
A
LA PLATA RIVER
N
0
-1000
-2000
-3000
-4000
-5000
-6000
DEPTH (m)
Current velocity
T2, V2
Guaíba river
L2
Camaquã river
Winds, salinity and
Temperature fields
+
Heat exchange
B
Tides
+
Low frequency water levels
T1, V1
L1
Current velocity
C
Naval / Praticagem
Stations
MV1
P1
S1
P3
P2
S8
S2
S7
S3
S6
S4
S5
MV2

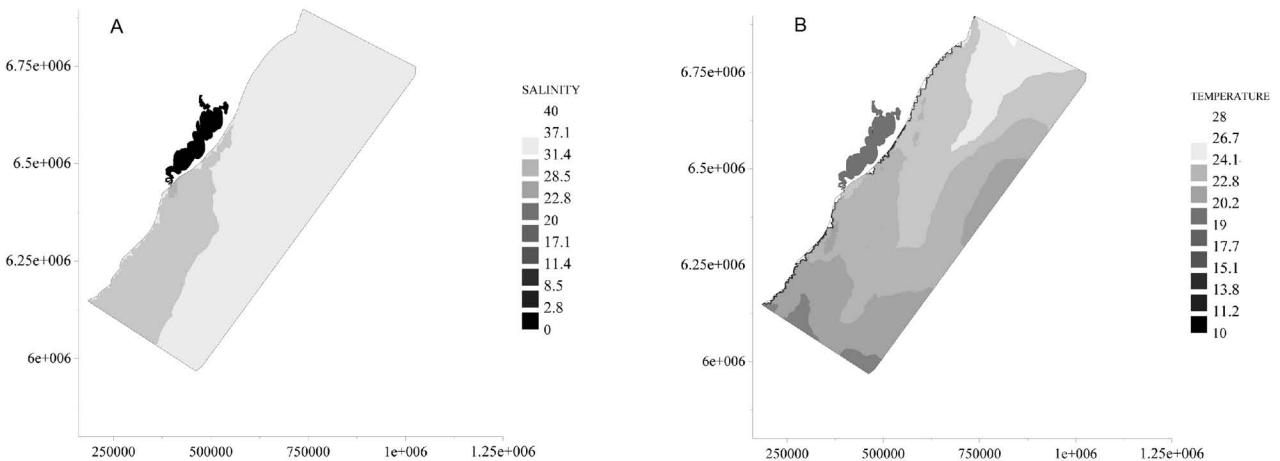
A
6.75e+006
6.5e+006
6.25e+006
6e+006
250000
500000
750000
1e+006
1.25e+006
SALINITY
40
37.1
31.4
28.5
22.8
20
17.1
11.4
8.5
2.8
0
B
6.75e+006
6.5e+006
6.25e+006
6e+006
250000
500000
750000
1e+006
1.25e+006
TEMPERATURE
28
26.7
24.1
22.8
20.2
19
17.7
15.1
13.8
11.2
10

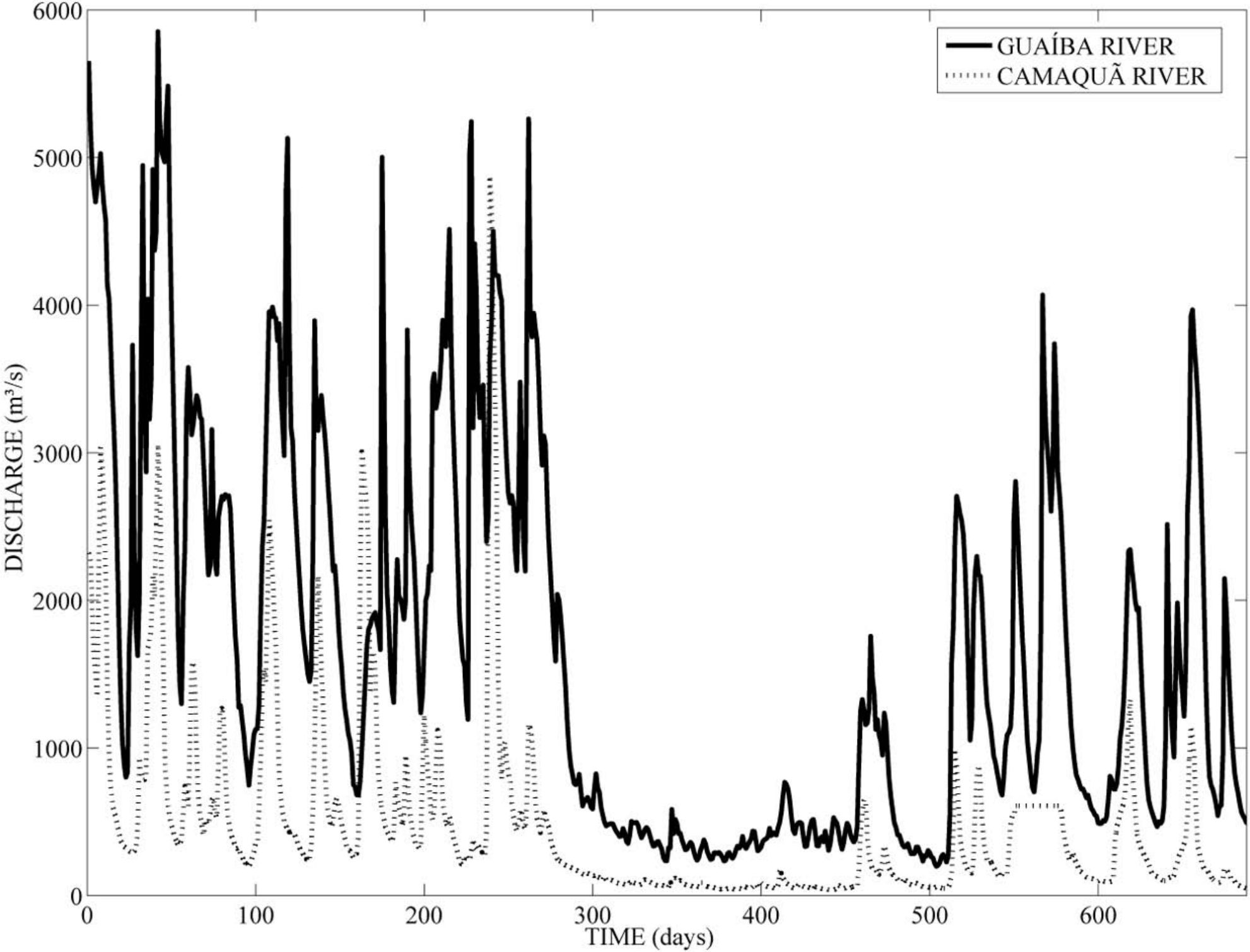
GUAÍBA RIVER
CAMAQUÃ RIVER
DISCHARGE (m³/s)
TIME (days)
0
1000
2000
3000
4000
5000
6000
0
100
200
300
400
500
600

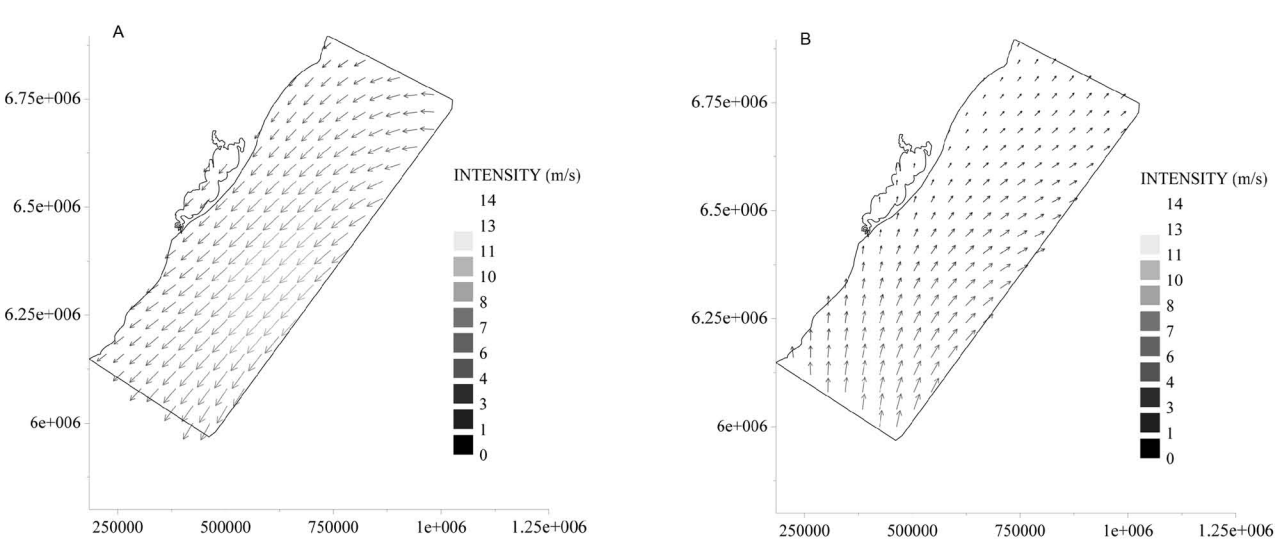
A
6.75e+006
6.5e+006
6.25e+006
6e+006
250000
500000
750000
1e+006
1.25e+006
INTENSITY (m/s)
14
13
11
10
8
7
6
4
3
1
0
B
6.75e+006
6.5e+006
6.25e+006
6e+006
250000
500000
750000
1e+006
1.25e+006
INTENSITY (m/s)
14
13
11
10
8
7
6
4
3
1
0

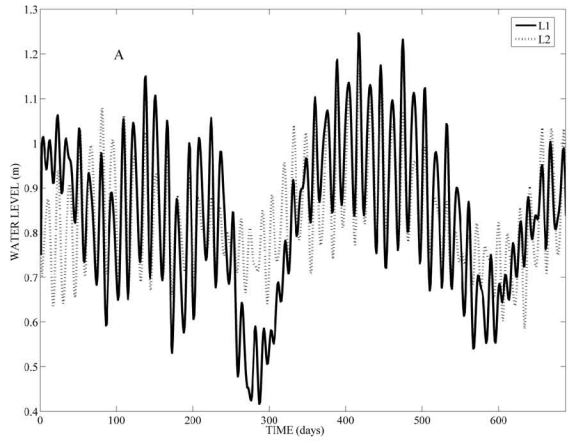
A
L1
L2
WATER LEVEL (m)
TIME (days)
1.3
1.2
1.1
1
0.9
0.8
0.7
0.6
0.5
0.4
0
100
200
300
400
500
600

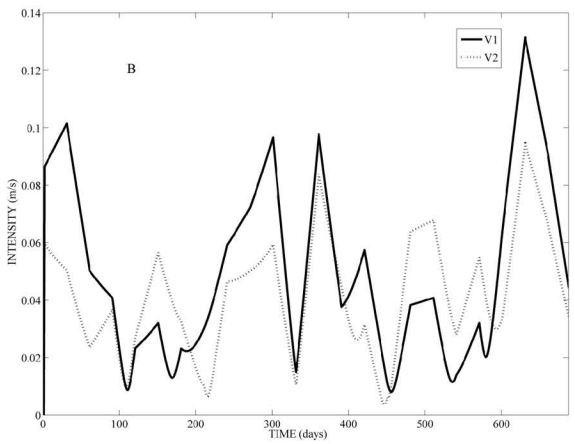
B
V1
V2
INTENSITY (m/s)
TIME (days)
0.14
0.12
0.1
0.08
0.06
0.04
0.02
0
0
100
200
300
400
500
600

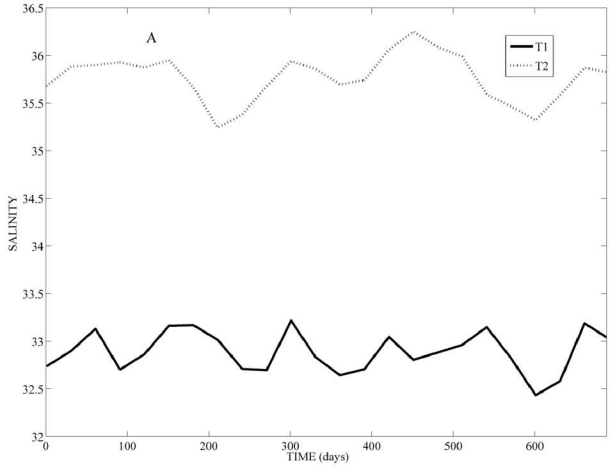
A
T1
T2
SALINITY
TIME (days)
36.5
36
35.5
35
34.5
34
33.5
33
32.5
32
0
100
200
300
400
500
600

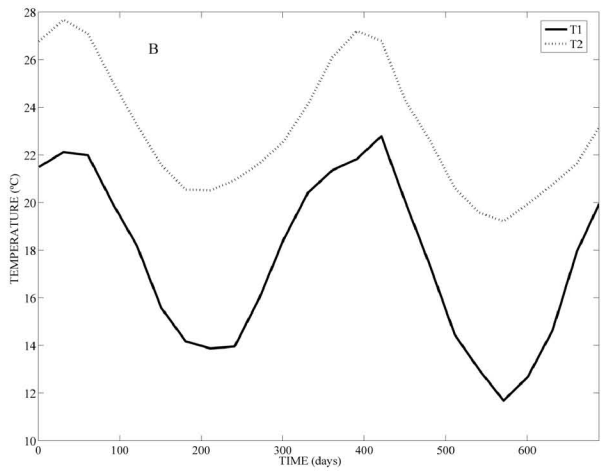
B
T1
T2
TEMPERATURE (°C)
TIME (days)
28
26
24
22
20
18
16
14
12
10
0
100
200
300
400
500
600

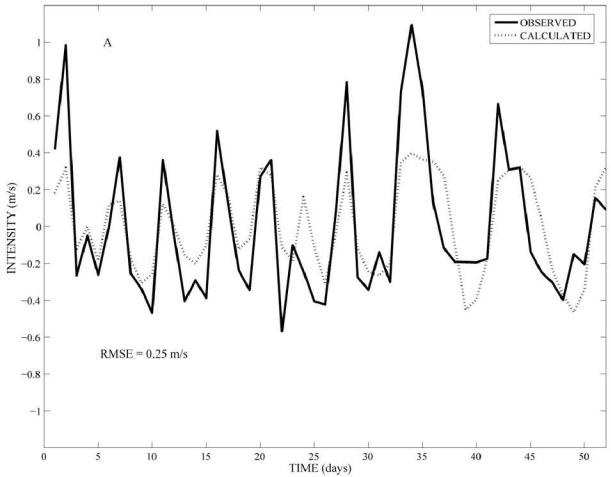
OBSERVED
CALCULATED
A
INTENSITY (m/s)
TIME (days)
RMSE = 0.25 m/s

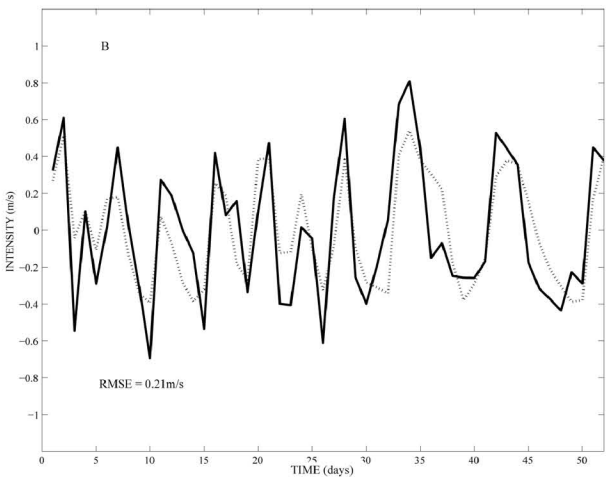
B
INTENSITY (m/s)
TIME (days)
RMSE = 0.21m/s

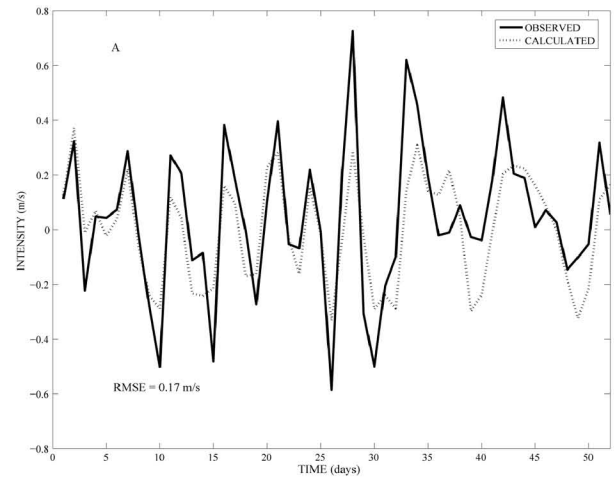
A
OBSERVED
CALCULATED
RMSE = 0.17 m/s
INTENSITY (m/s)
TIME (days)

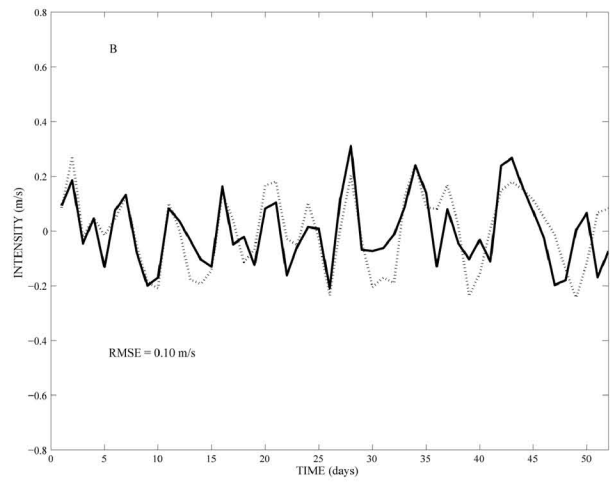
B
RMSE = 0.10 m/s
INTENSITY (m/s)
TIME (days)

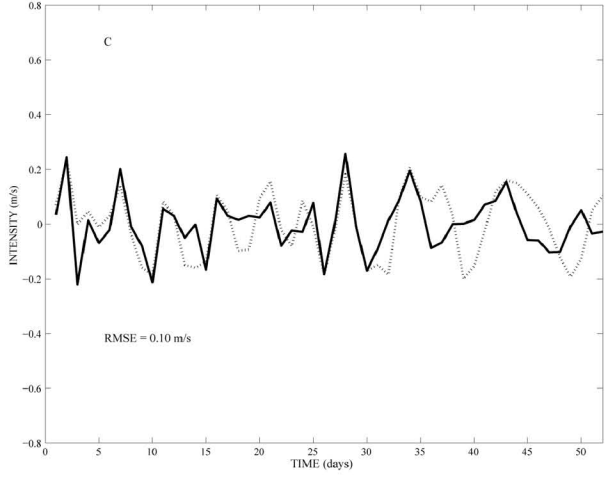
C
RMSE = 0.10 m/s
INTENSITY (m/s)
TIME (days)

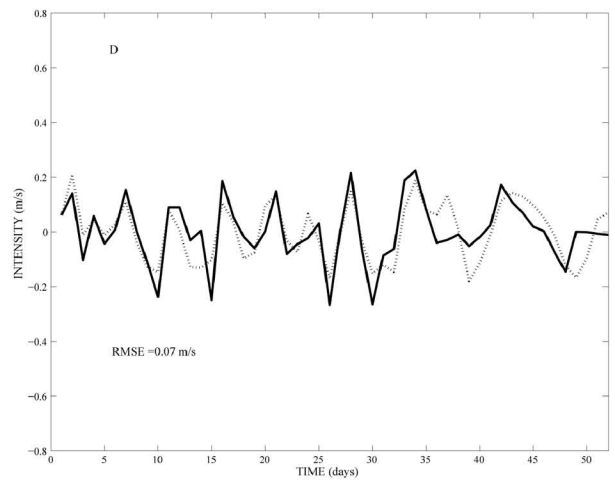
D
RMSE =0.07 m/s
INTENSITY (m/s)
TIME (days)

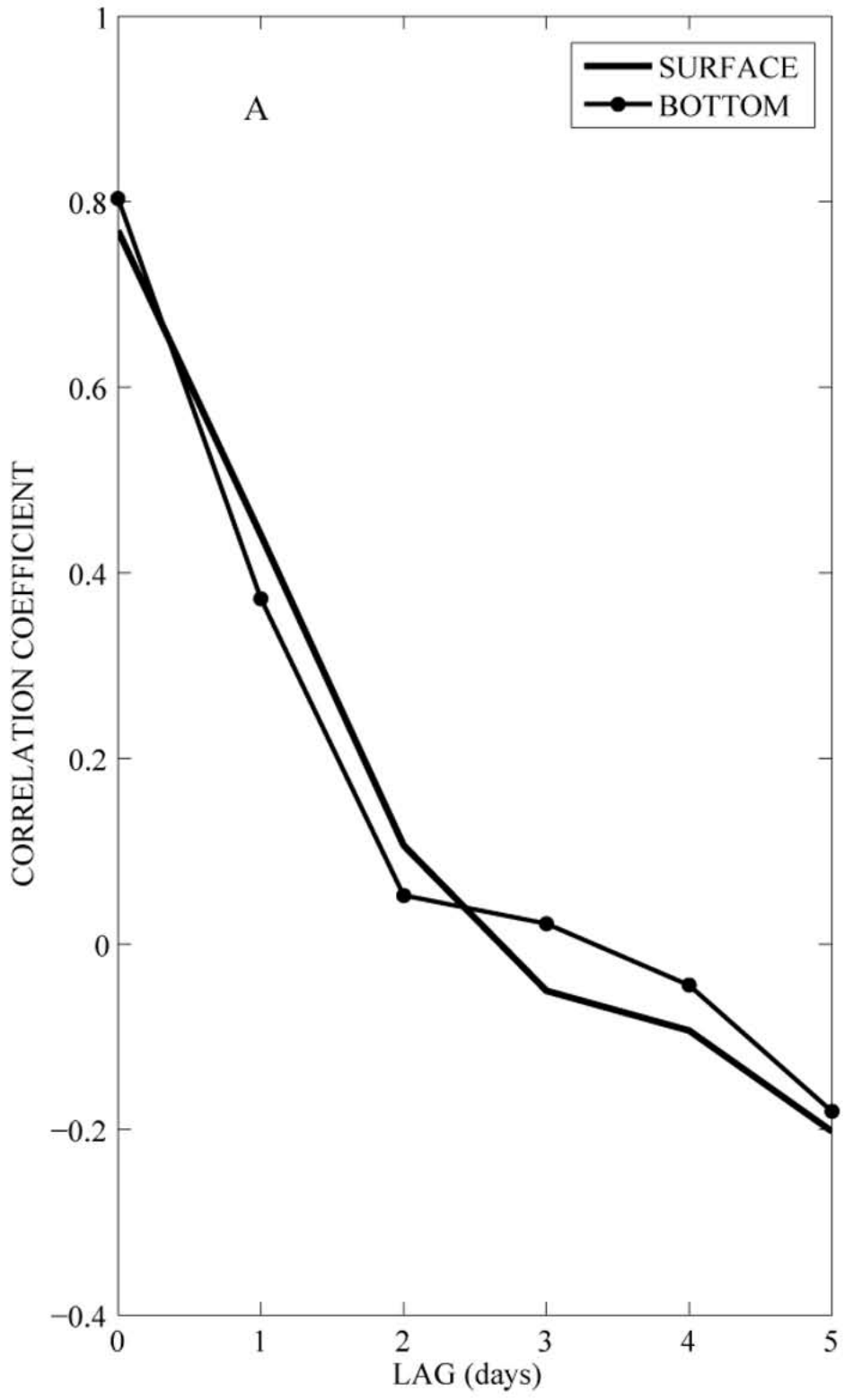
A
SURFACE
BOTTOM
CORRELATION COEFFICIENT
LAG (days)
1
0.8
0.6
0.4
0.2
0
−0.2
−0.4
0
1
2
3
4
5

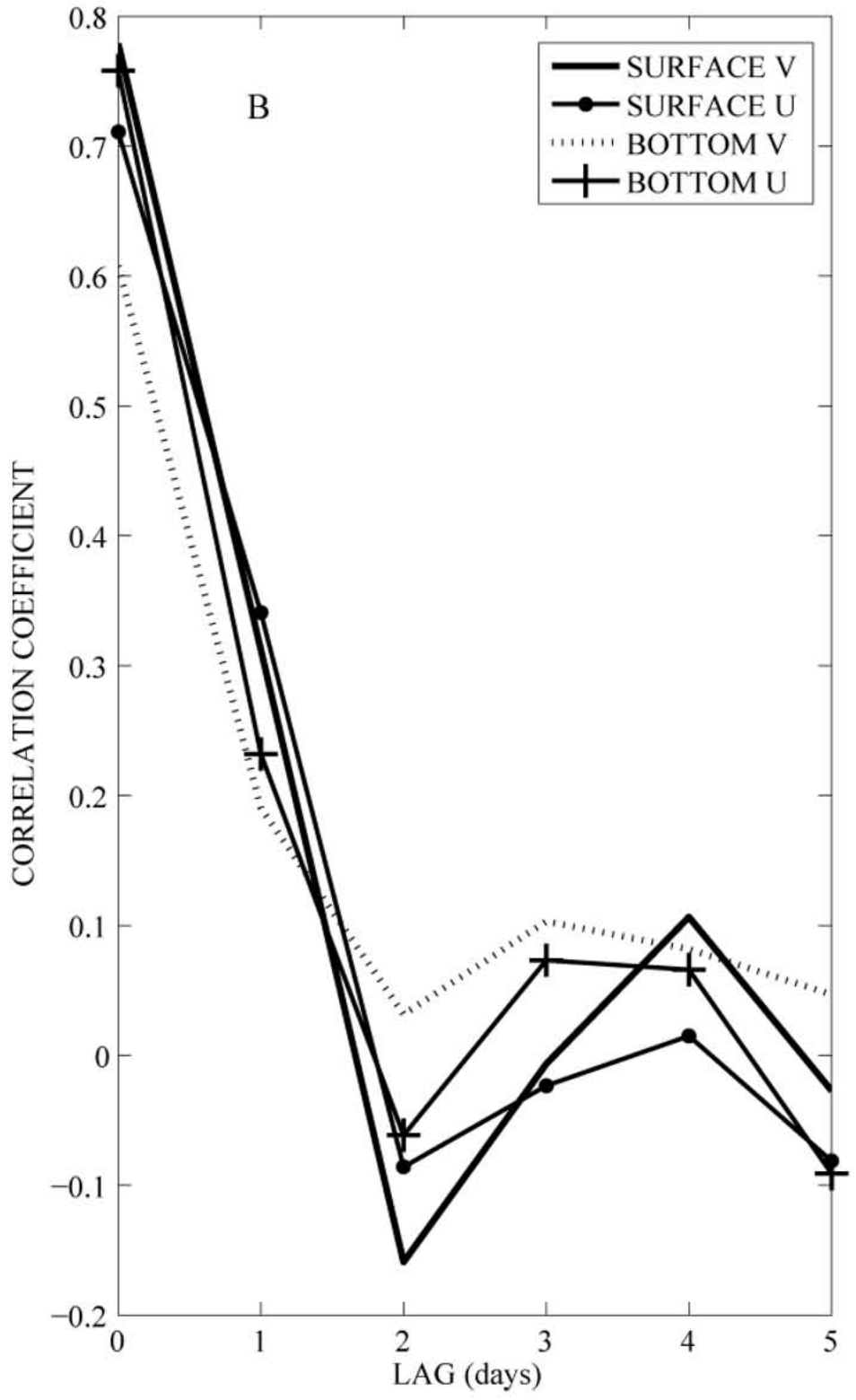
B
SURFACE V
SURFACE U
BOTTOM V
BOTTOM U
CORRELATION COEFFICIENT
LAG (days)
0.8
0.7
0.6
0.5
0.4
0.3
0.2
0.1
0
−0.1
−0.2
0
1
2
3
4
5

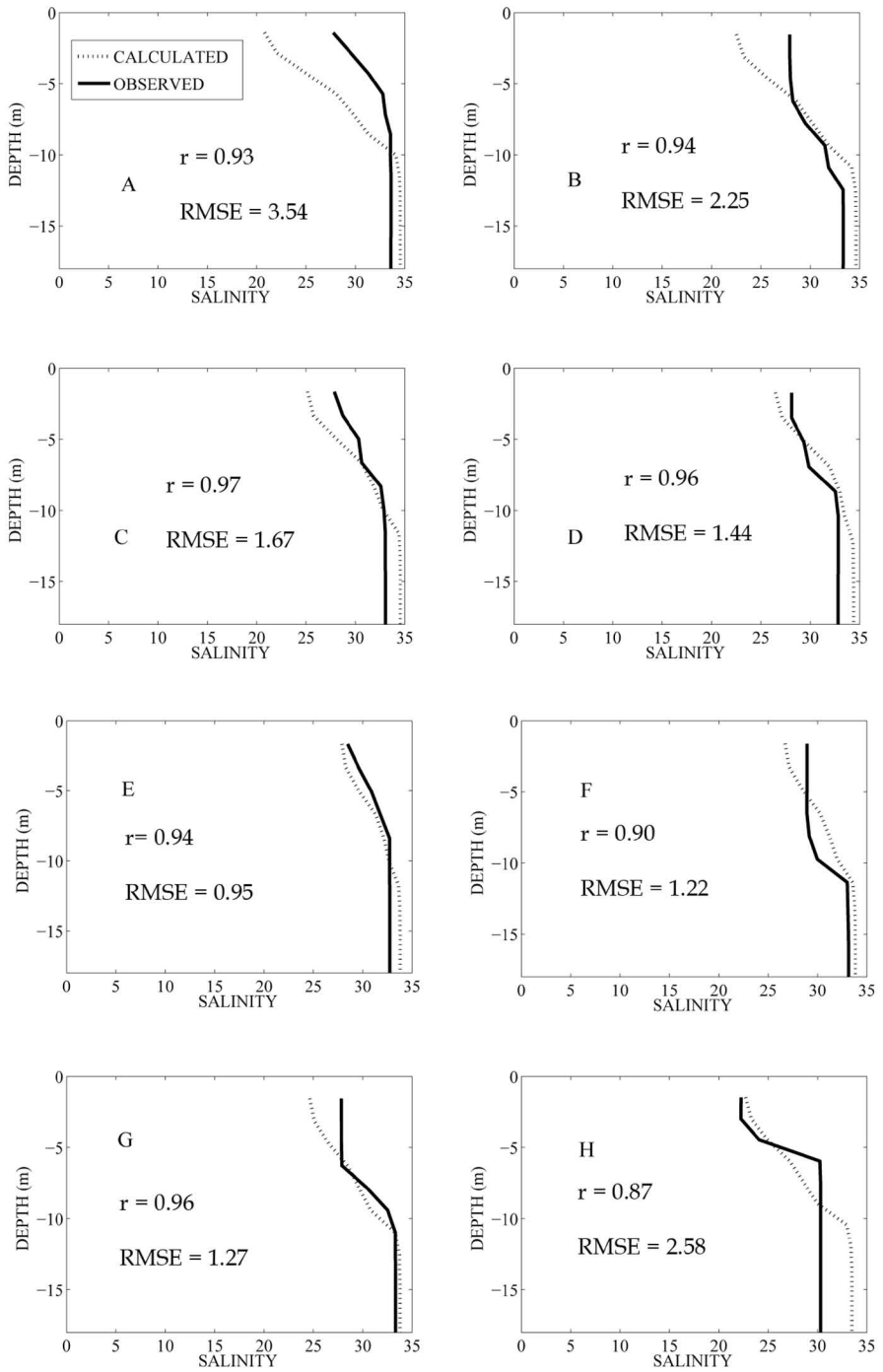
CALCULATED
OBSERVED
A
r = 0.93
RMSE = 3.54
B
r = 0.94
RMSE = 2.25
C
r = 0.97
RMSE = 1.67
D
r = 0.96
RMSE = 1.44
E
r= 0.94
RMSE = 0.95
F
r = 0.90
RMSE = 1.22
G
r = 0.96
RMSE = 1.27
H
r = 0.87
RMSE = 2.58
DEPTH (m)
SALINITY

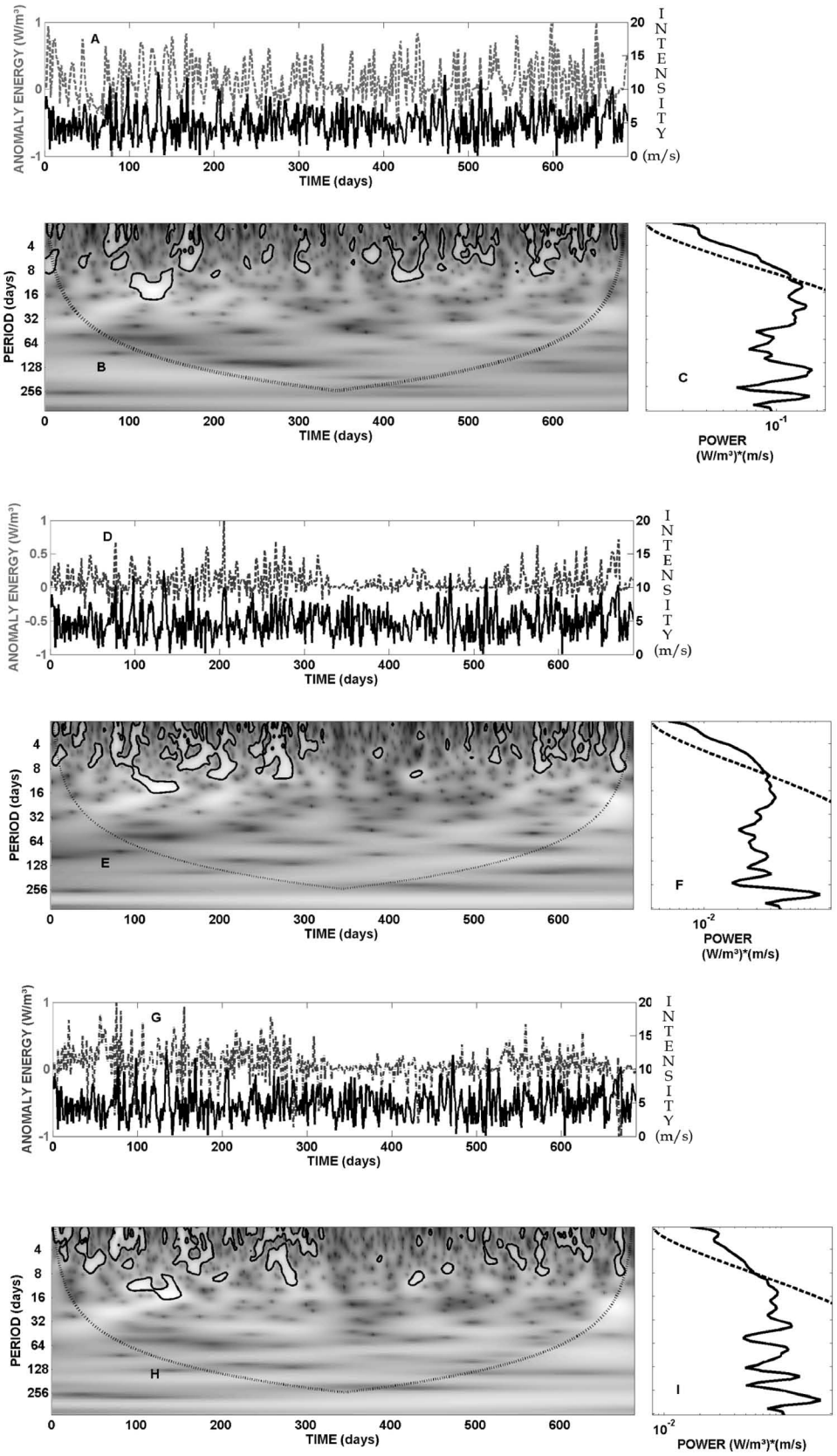
A
ANOMALY ENERGY (W/m³)
INTENSITY (m/s)
TIME (days)
B
PERIOD (days)
TIME (days)
C
POWER (W/m³)*(m/s)
D
ANOMALY ENERGY (W/m³)
INTENSITY (m/s)
TIME (days)
E
PERIOD (days)
TIME (days)
F
POWER (W/m³)*(m/s)
G
ANOMALY ENERGY (W/m³)
INTENSITY (m/s)
TIME (days)
H
PERIOD (days)
TIME (days)
I
POWER (W/m³)*(m/s)

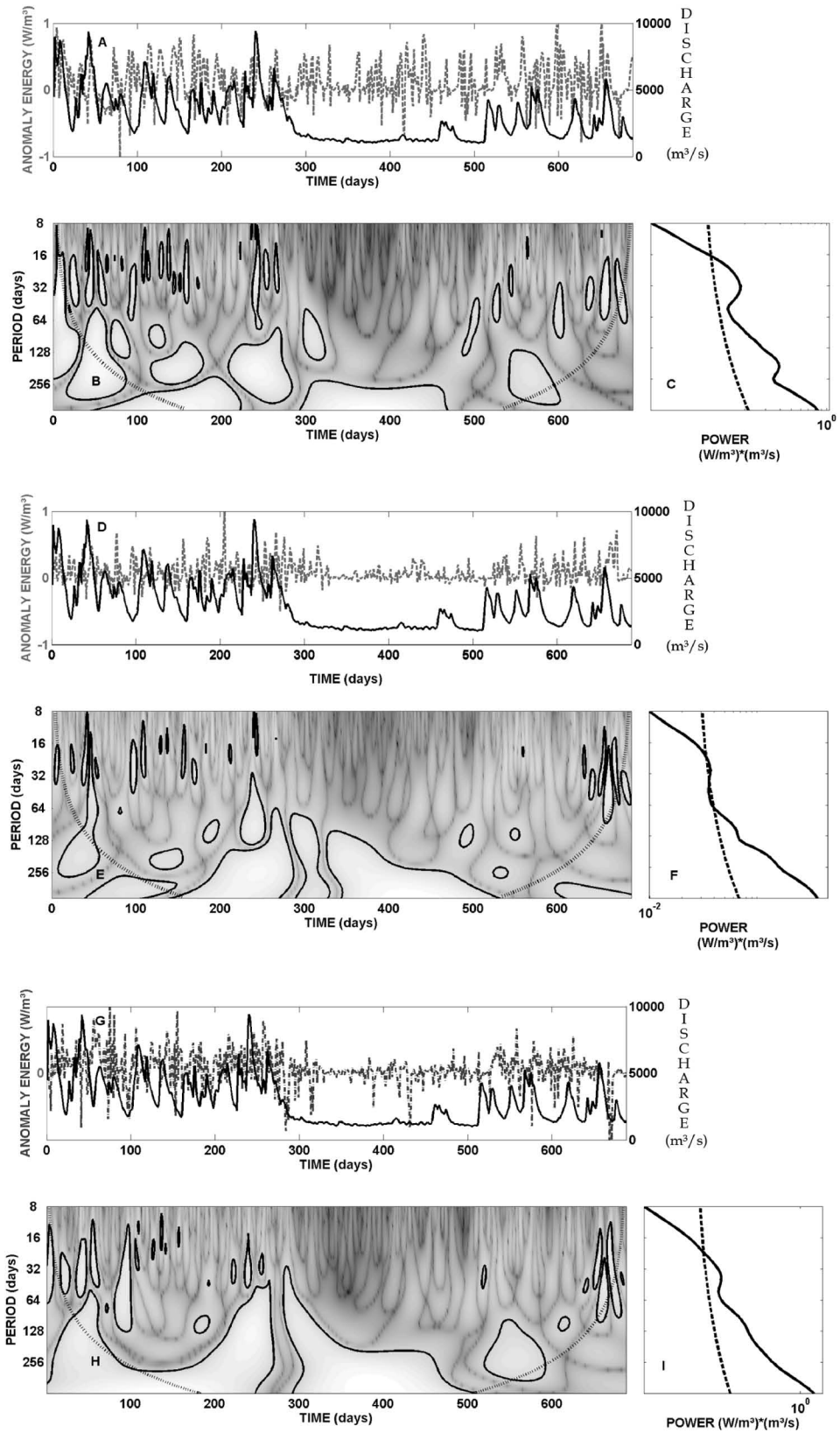
A
ANOMALY ENERGY (W/m³)
DISCHARGE (m³/s)
TIME (days)
B
PERIOD (days)
C
POWER (W/m³)*(m³/s)
D
E
F
G
H
I

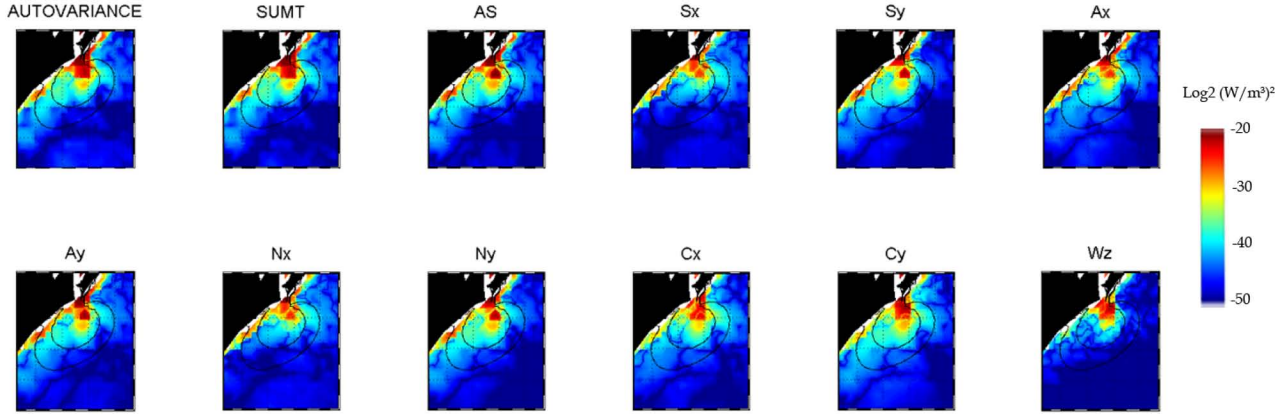
AUTOVARIANCE
SUMT
AS
Sx
Sy
Ax
Ay
Nx
Ny
Cx
Cy
Wz
Log2 (W/m³)²
-20
-30
-40
-50

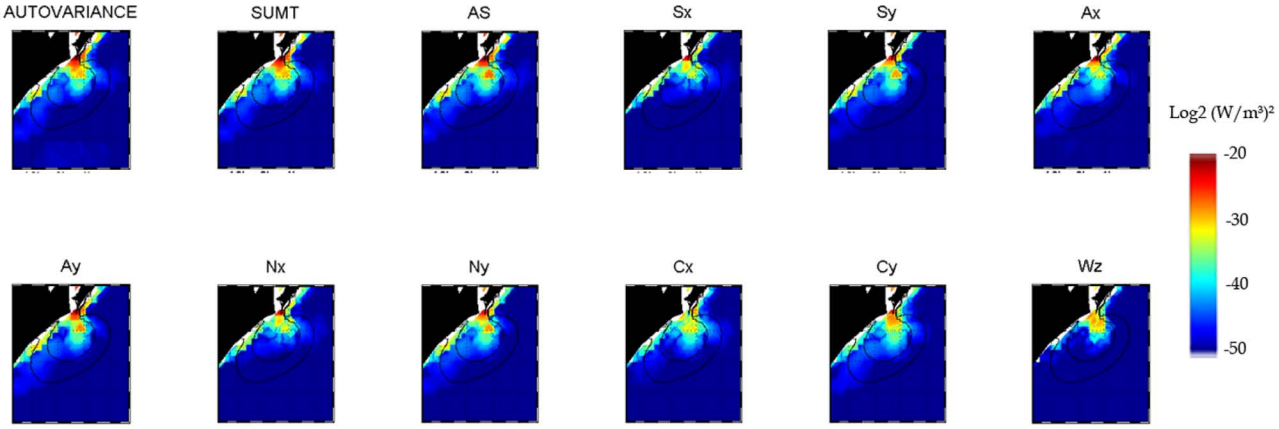
AUTOVARIANCE
SUMT
AS
Sx
Sy
Ax
Ay
Nx
Ny
Cx
Cy
Wz
Log2 (W/m³)²
-20
-30
-40
-50

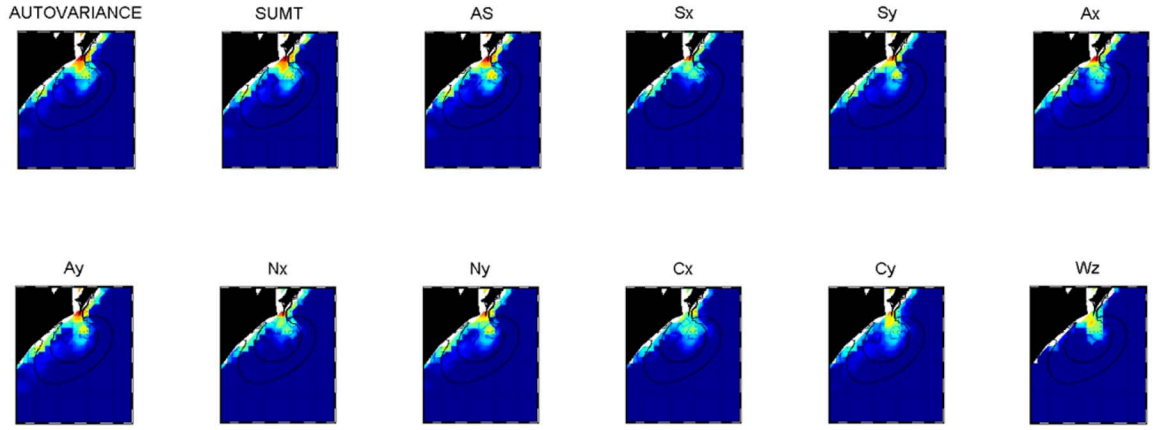
AUTOVARIANCE
SUMT
AS
Sx
Sy
Ax
Ay
Nx
Ny
Cx
Cy
Wz
Log2 (W/m³)²
-20
-30
-40
-50

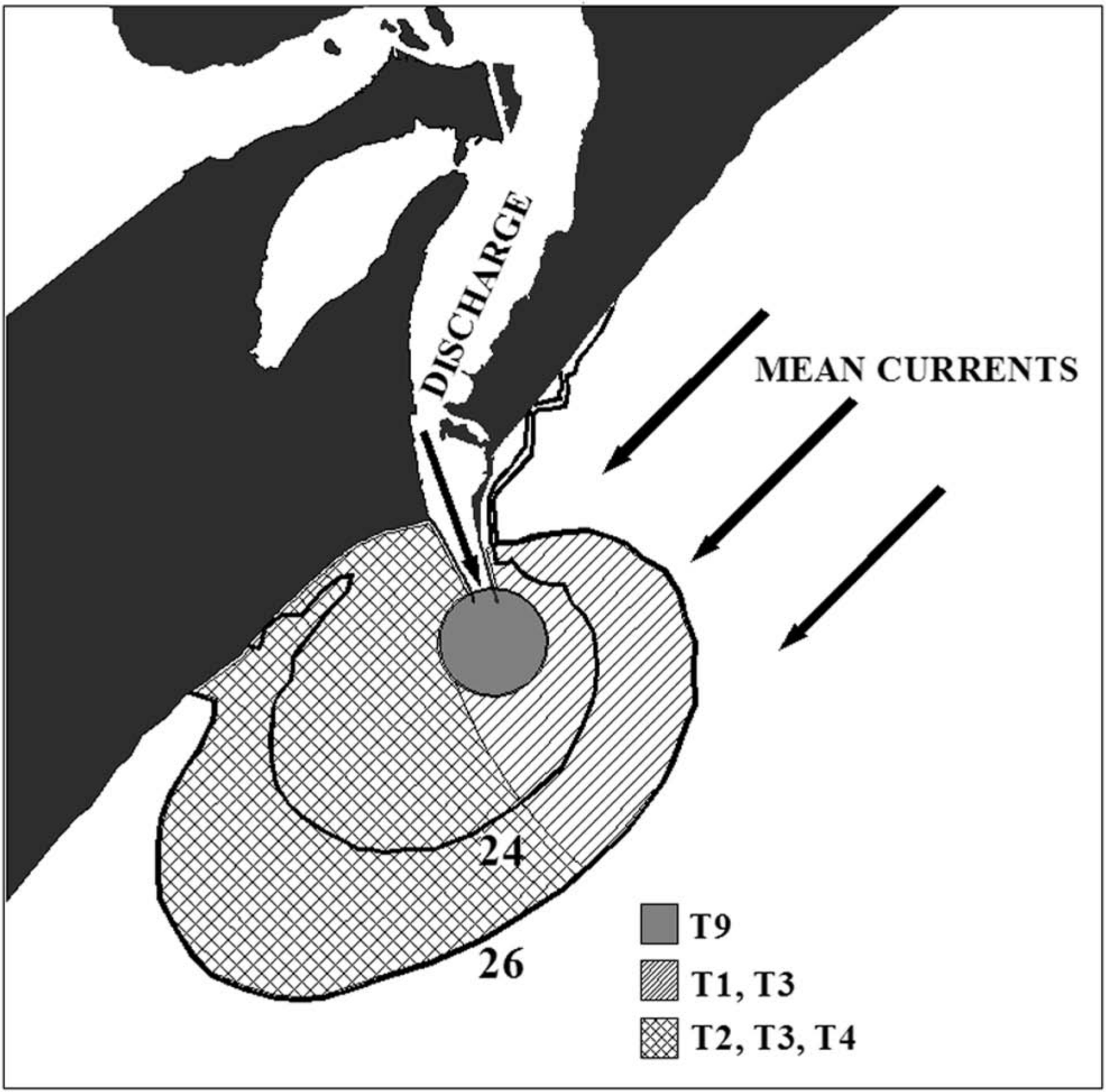
DISCHARGE
MEAN CURRENTS
24
26
T9
T1, T3
T2, T3, T4

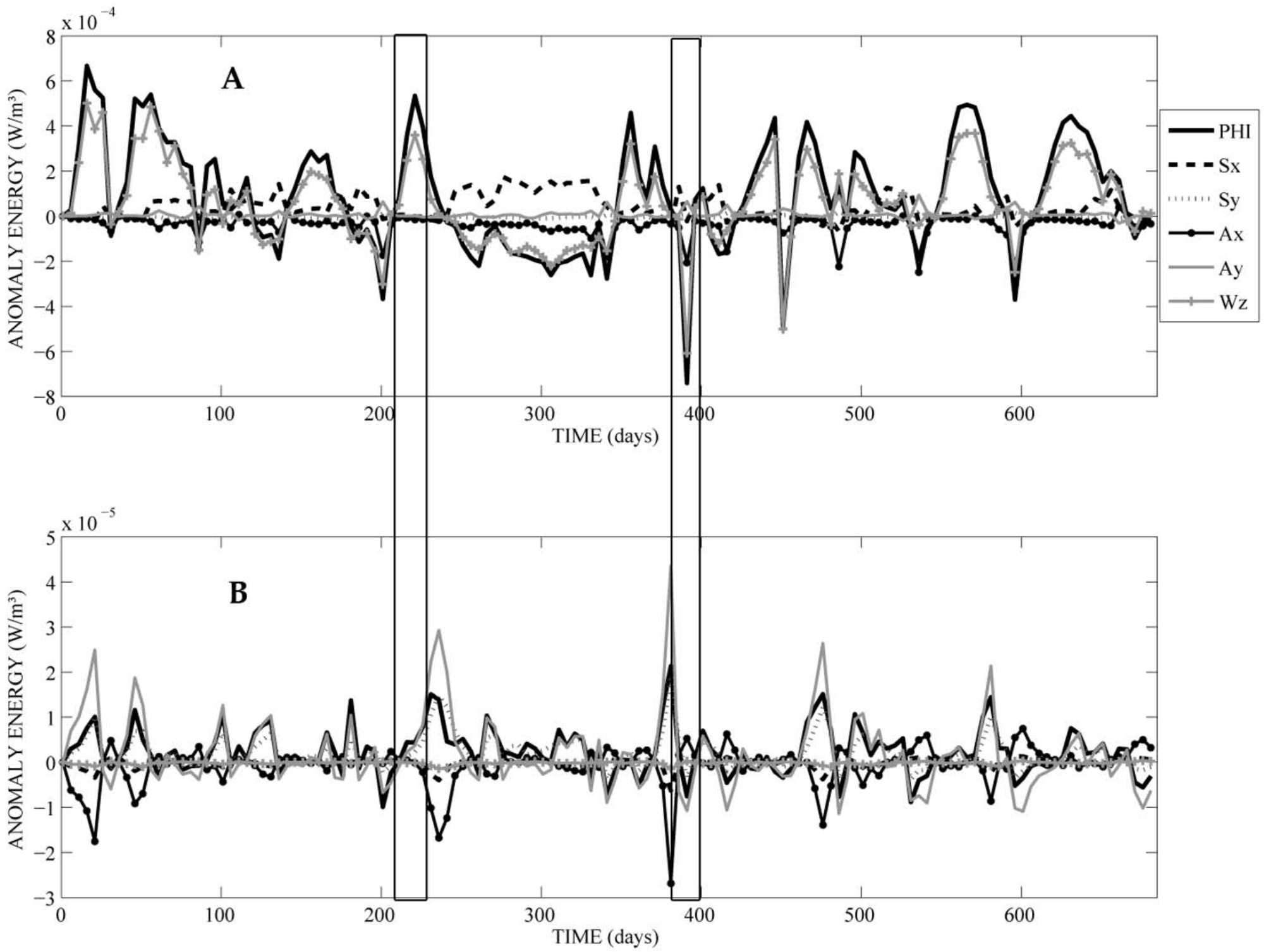
x 10^-4
A
ANOMALY ENERGY (W/m³)
TIME (days)
PHI
Sx
Sy
Ax
Ay
Wz
x 10^-5
B
ANOMALY ENERGY (W/m³)
TIME (days)

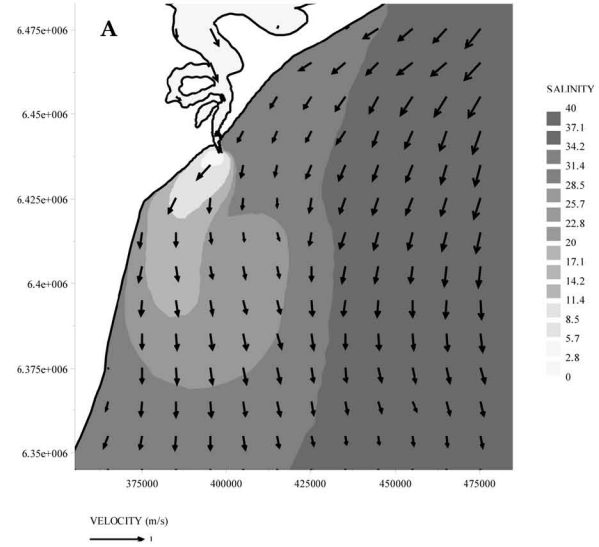
A
6.475e+006
6.45e+006
6.425e+006
6.4e+006
6.375e+006
6.35e+006
375000
400000
425000
450000
475000
SALINITY
40
37.1
34.2
31.4
28.5
25.7
22.8
20
17.1
14.2
11.4
8.5
5.7
2.8
0
VELOCITY (m/s)
1

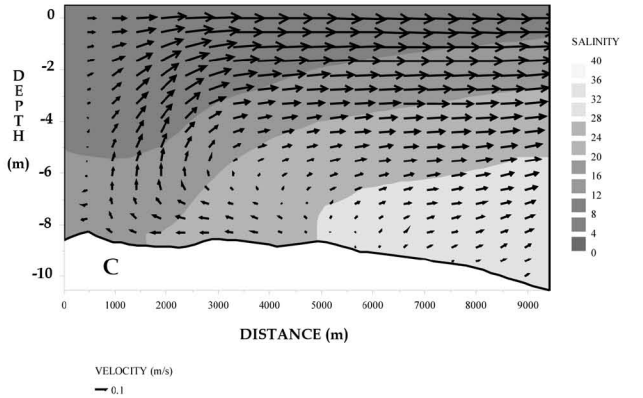
C
DEPTH (m)
0
-2
-4
-6
-8
-10
0
1000
2000
3000
4000
5000
6000
7000
8000
9000
DISTANCE (m)
SALINITY
40
36
32
28
24
20
16
12
8
4
0
VELOCITY (m/s)
0.1

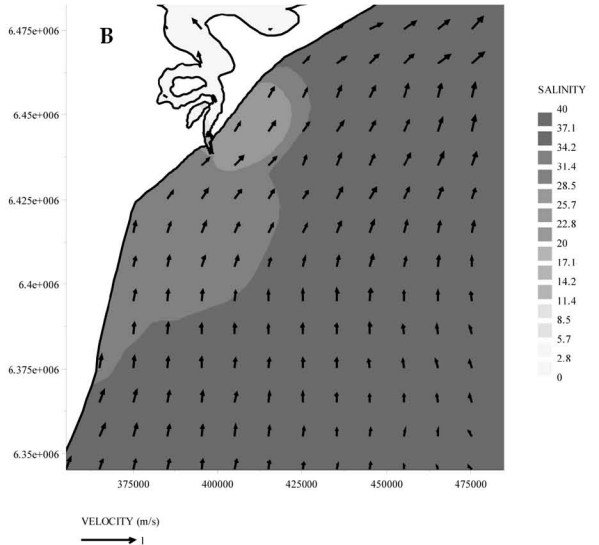
B
6.475e+006
6.45e+006
6.425e+006
6.4e+006
6.375e+006
6.35e+006
375000
400000
425000
450000
475000
SALINITY
40
37.1
34.2
31.4
28.5
25.7
22.8
20
17.1
14.2
11.4
8.5
5.7
2.8
0
VELOCITY (m/s)
1

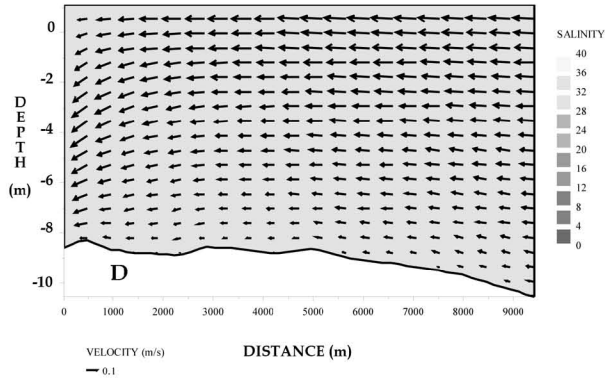
D
DEPTH (m)
0
-2
-4
-6
-8
-10
0
1000
2000
3000
4000
5000
6000
7000
8000
9000
DISTANCE (m)
SALINITY
40
36
32
28
24
20
16
12
8
4
0
VELOCITY (m/s)
0.1